
Slot Order Matters for Compositional Scene Understanding

Patrick Emami^{1,2}

Pan He²

Sanjay Ranka²

Anand Rangarajan²

¹National Renewable Energy Lab

²University of Florida

patrickemami@gmail.com, pan.he@ufl.edu, {ranka,anand}@cise.ufl.edu

Abstract

Empowering agents with a compositional understanding of their environment is a promising next step toward solving long-horizon planning problems. On the one hand, we have seen encouraging progress on variational inference algorithms for obtaining sets of object-centric latent representations (“slots”) from unstructured scene observations. On the other hand, generating scenes from slots has received less attention, in part because it is complicated by the lack of a canonical object order. A canonical object order is useful for learning the object correlations necessary to generate physically plausible scenes similar to how raster scan order facilitates learning pixel correlations for pixel-level autoregressive image generation. In this work, we address this lack by learning a fixed object order for a hierarchical variational autoencoder with a single level of autoregressive slots and a global scene prior. We cast autoregressive slot inference as a set-to-sequence modeling problem. We introduce an auxiliary loss to train the slot prior to generate objects in a fixed order. During inference, we align a set of inferred slots to the object order obtained from a slot prior rollout. To ensure the rolled out objects are meaningful for the given scene, we condition the prior on an inferred global summary of the input. Experiments on compositional environments and ablations demonstrate that our model with global prior, inference with aligned slot order, and auxiliary loss achieves state-of-the-art sample quality.

1 Introduction

Humans can look at a scene and parse what objects are present and how they relate to each other seemingly effortlessly. We can also imagine highly complex scenes based on the objects we perceive. To achieve this, our visual system segregates raw perceptions into meaningful entities, binds these entities to object-centric representations (e.g., *object files* [36]), and infers object relationships [4; 64]. A major goal of artificial intelligence is to develop agents capable of such human-like compositional scene understanding [5; 40; 82]. For example, this would enable robots to reason about the effects of their actions on different objects which is essential for long-term planning and decision-making.

Variational autoencoders (VAEs) [38; 59] are a natural model family for compositional scene understanding since they offer a principled unsupervised learning framework based on scene inference and generation [78]. However, inferring composable and modular representations from noisy observations of multi-object scenes and generating scenes by composing these representations remains challenging. Inference requires segregating the input into object-centric entities and binding them to a set of latent variables (i.e., the *binding problem* [22]). This appears to be fundamentally difficult for VAEs that encode observations into monolithic unstructured representations (e.g., DALL-E [56]) or into fixed-size grids of symbolic variables [17; 10; 46]. Other VAEs instead represent observations as

mixture distributions whose components are in correspondence with a set of object-centric latent variables, or “slots”. These *slot VAEs* have demonstrated encouraging segmentation and disentanglement performance on static [6; 21; 15; 16; 14], multi-view [41; 65; 77; 76; 42], and dynamic visual scenes [74; 70; 45; 79; 11; 35; 83]. However, slot VAEs generate low-quality scenes [15; 16; 32].

Compositional scene generation is difficult because it requires learning how objects are correlated in the data. For example, consider an image dataset of cars driving on a road. A failure to learn the spatial correlation between the cars, sky, and road leads to generating physically implausible scenes with flying cars or two cars occupying the same physical space. Learning multi-object correlations is uniquely challenging because objects have no *canonical ordering*. In general, it is easier to learn correlations between variables when the variable order is fixed, e.g., to a canonical order. Consider pixel-level autoregressive models based on raster scan order [60; 67; 53; 9; 8]. These models essentially learn an autoregressive distribution for each pixel conditioned on all previous pixels in the order. This enables the n^{th} distribution to learn correlations between the n^{th} pixel and the previous $n - 1$ pixels across training images, resulting in a highly expressive image density. VAEs that autoregressively model slots have evidently ignored the issue of order by their use of random and arbitrary orders for inference [15; 16]. Others simply assume slots are independent and cannot generate coherent scenes [21; 14]. We attribute the poor sample quality of slot VAEs to their limited ability to learn object correlations.

In this work, we propose to address the lack of a canonical object order by *learning* a fixed object order, which we use to estimate complex correlations and achieve high-quality scene generation. We cast slot inference as a set-to-sequence modeling problem; specifically, we impose a learned object order on a randomly ordered segregation slot posterior to obtain an autoregressive slot posterior. To learn an object order suitable for high-quality scene generation and to avoid the complexity of introducing discrete latent variables for order inference, we use an implicit approach that is generative in nature. In detail, we introduce a two-level hierarchical slot VAE with a level of autoregressive slot variables conditioned on a global scene-level variable. We use the global prior to aid with learning the object order and also to increase the expressiveness of the autoregressive distributions for learning higher-order correlations. We introduce an auxiliary loss that trains the slot prior to use a fixed object generation order. During set-to-sequence slot inference, the autoregressive slot order is aligned to the object order extracted from a slot prior *imagination rollout*. We condition the prior on an inferred global summary of the input to ensure the rolled out object order is meaningful for inference on the given observation. Our experiments show that our model, SRI (Segregate, Relate, Imagine), achieves state-of-the-art generative performance among slot VAEs across multiple compositional environments. Detailed ablation studies demonstrate that the global prior, inference with aligned slot order, and auxiliary loss all work in concert to achieve the best performance, suggesting that *slot order matters* for compositional scene understanding.

2 Related Work

Slot VAEs: Slot VAEs are essentially VAEs with a set of K latent variables and a mixture model observation likelihood. IODINE [21] and EfficientMORL (EMORL) [14] use iterative inference to refine a randomly ordered posterior distribution over slots; EMORL also initializes iterative refinement with probabilistic slot attention [47]. Neither are capable of coherent scene generation due to using independent slot priors. GENESIS-v2 (GENv2) [16] also infers a randomly ordered slot posterior (via differentiable clustering) yet has an autoregressive slot prior able to capture object correlations. However, GENv2 assumes inferred slots are randomly ordered (i.e., uncorrelated) which hurts the sample quality of generated scenes. GENESIS (GEN) [15]) initially proposed the autoregressive prior and uses sequential attention to segregate observations following an arbitrary object order; however, arbitrarily ordered attention works poorly on complex environments [16]. By contrast, SRI aligns its autoregressive slots to a learned, fixed object order and has a global prior for expressive modeling of higher-order correlations. Other related VAEs for scene generation [2; 73] make simplifying independence assumptions that prevent them from scaling to non-trivial environments.

Spatial-symbolic VAEs: Generative Neurosymbolic Machine (GNM) [32] is a VAE that combines a global scene-level prior with symbolic latent variables for compositional scene understanding. SRI is the first to explore using a global prior in the context of slot VAEs and for learning slot order. GNM’s symbolic variables differ from slots in that they have explicit semantic meaning (e.g., as bounding box coordinates) and are arranged as a fixed-size grid [17; 10; 46]. We demonstrate in this work that

GNM fails to discover objects in environments where objects vary widely in size and/or occlude each other heavily. The related model GSGN [12] attempts to learn part-whole object hierarchies but has the same limited symbolic variables as GNM.

Compositional GANs: Certain GANs can compose noise variables to generate scenes with object-level controllability [68; 51; 44; 13; 52; 30; 3]; however, they are fundamentally limited without a mechanism for addressing inference (i.e., the binding problem). Interestingly, RELATE [13] and GANformer2 [3] also learn a good generation order, which lends support to our claim that aligning the slot order to a fixed object order improves correlation estimation (i.e., that *slot order matters*).

Set-to-sequence modeling: A variety of methods have been proposed for sequential modeling where the input data has no canonical order (e.g., it is an arbitrarily ordered set) but the output is ordered, starting from the seminal work of Vinyals et al. [72]. A popular approach is to use Pointer Networks [71] or to make use of continuous relaxations of permutations [1; 48; 81; 43] or differentiable sorting [24]. See Jurewicz & Derczynski [33] for a survey. Unlike these methods, we *implicitly* learn a slot order using the slot prior to bias learning towards orders useful for high-quality scene generation and to avoid the complexity of discrete order inference.

3 Segregate, Relate, Imagine (SRI)

The statistical problem we are concerned with is fitting the underlying data-generating process $p(\mathcal{D})$ for an unlabeled dataset \mathcal{D} of i.i.d. scene observations $\mathbf{x} \in \mathbb{R}^{N \times C}$ containing multiple objects. In this work we restrict our focus to collections of RGB images so that $N = H \times W$ and $C = 3$. Like previous slot VAEs, we assume that the marginal likelihood for an image $p(\mathbf{x})$ is augmented with K slots $\mathbf{z}_k \in \mathbb{R}^z$ [21; 15; 16; 14]. Typically, K is chosen to be larger than the number of objects in any given scene in \mathcal{D} . We introduce a latent variable $\mathbf{s} \in \mathbb{R}^s$ to serve as a hierarchical prior on the slots and whose posterior distribution summarizes global statistics such as higher-order correlations between objects. This gives the following joint distribution: $p(\mathbf{x}, \mathbf{z}_{\pi_{1:K}}, \mathbf{s})$, where $\pi_{1:K} := \pi_1, \pi_2, \dots, \pi_K$ is some permutation of the integers $\{1, \dots, K\}$. We use this notation to make slot order explicit. In what follows, θ are neural net parameters for prior distributions and ψ, ϕ are neural net parameters for variational posterior distributions. Following common practice all latents are Gaussian with diagonal covariance.

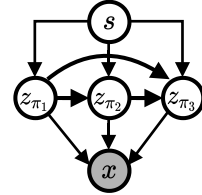


Figure 1: The SRI generative model ($K = 3$).

3.1 Generative Model

SRI factorizes the joint distribution into a two-level hierarchy where we assume the observation \mathbf{x} , when conditioned on the slots, is independent of the scene variable (Figure 1):

$$p_{\theta}(\mathbf{x}, \mathbf{z}_{\pi_{1:K}}, \mathbf{s}) = p(\mathbf{s})p_{\theta}(\mathbf{z}_{\pi_{1:K}} | \mathbf{s})p_{\theta}(\mathbf{x} | \mathbf{z}_{\pi_{1:K}}). \quad (1)$$

For $p(\mathbf{s})$ we use a standard Gaussian. The slot prior is autoregressive with order $\pi_{1:K}$:

$$p_{\theta}(\mathbf{z}_{\pi_{1:K}} | \mathbf{s}) = p_{\theta}(\mathbf{z}_{\pi_1} | \mathbf{s}) \prod_{k=2}^K p_{\theta}(\mathbf{z}_{\pi_k} | \mathbf{z}_{\pi_{1:k-1}}, \mathbf{s}). \quad (2)$$

Unlike the autoregressive slot prior used by GEN and GENv2, our prior is conditioned on \mathbf{s} which increases its expressiveness for modeling higher-order correlations. The conditional image likelihood can be a pixel-wise Gaussian (left) or Mixture-of-Gaussians (right):

$$p_{\theta}(\mathbf{x} | \mathbf{z}_{\pi_{1:K}}) := \prod_{i=1}^N \mathcal{N}\left(\sum_{k=1}^K m_{i,k} x_{i,k}, \sigma^2\right) \quad \text{or} \quad \prod_{i=1}^N \sum_{k=1}^K m_{i,k} \mathcal{N}(x_{i,k}, \sigma^2), \quad (3)$$

where $x_{i,k} \in \mathbb{R}^C$ is an RGB pixel, $m_{i,k} \in [0, 1]$ is a mask, and σ^2 is a shared variance. While a Gaussian likelihood is easier to optimize, the Mixture-of-Gaussians can achieve better segmentation and reconstruction quality [6; 21; 15; 16]. We consider both in our experiments. To facilitate comparing SRI with previous slot VAEs, we use the same spatial broadcasting decoder (SBD) [75; 14; 16] to map each slot \mathbf{z}_{π_k} to mixture components (x_k, m_k) , leaving the exploration of recently proposed advanced compositional decoders for future work [63]. The autoregressive prior $p_{\theta}(\mathbf{z}_{\pi_{1:K}} |$

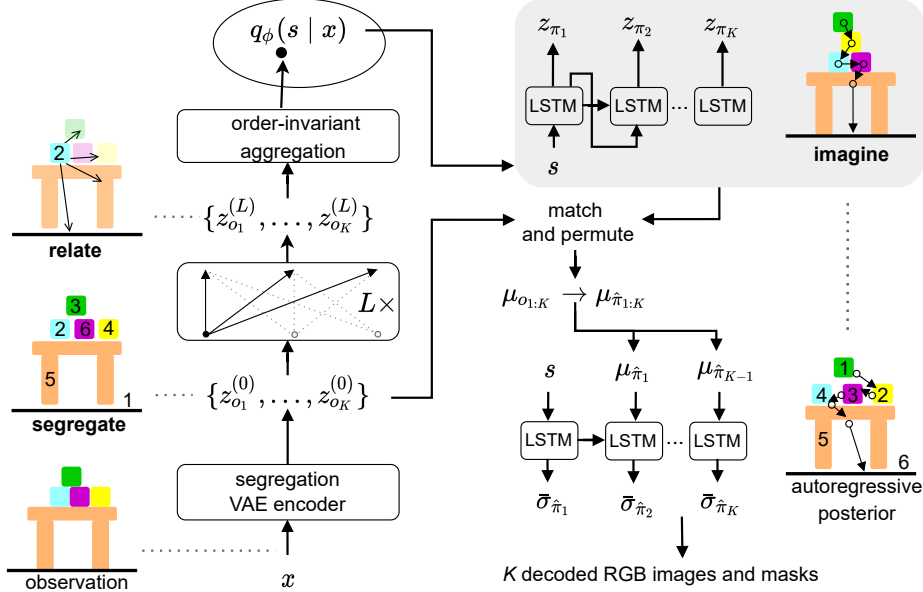


Figure 2: **Segregate, Relate, Imagine (SRI)**. SRI learns a fixed object generation order which we extract for autoregressive inference. This helps the prior and posterior autoregressive distributions for the k^{th} slot learn correlations with respect to the previous $k - 1$ slots in the learned order. In the encoding pass, SRI first segregates the observation \mathbf{x} (e.g., using GENv2 [16]) and obtains randomly ordered slots $\mathbf{z}_{o_{1:K}}$. An order-invariant relational embedding of this set is encoded into a global posterior $q_\phi(\mathbf{s} | \mathbf{x})$. An imagination rollout conditioned on a sample \mathbf{s} gives us slots with fixed order $\pi_{1:K}$. We extract order $\hat{\pi}_{1:K}$ by matching the randomly ordered and imagined slots, then transform the segregation posterior into an autoregressive posterior with order $\hat{\pi}_{1:K}$ by predicting correlated variances $\bar{\sigma}_{\hat{\pi}_{1:K}}$. The autoregressive slots $\mathbf{z}_{\hat{\pi}_{1:K}}$ are decoded into RGB images and masks.

\mathbf{s}) is implemented with an LSTM [28]. We project the scene variable via $\mathbf{W}_s^\top \mathbf{s}$, $\mathbf{W}_s \in \mathbb{R}^{s \times z}$ followed by a nonlinear activation function to pass as input to $p_\theta(\mathbf{z}_{\pi_1} | \mathbf{s})$. Two shared linear layers are used to map the K LSTM outputs to Gaussian means and variances.

To generate an image, we first sample from the scene prior and then sample sequentially from the autoregressive slot prior. The K sampled slots are passed to the SBD to predict masks and RGB images. The K masks are normalized with a softmax before the sum aggregation in Eq. 3.

3.2 Set-to-Sequence Inference

During inference, we infer variational posteriors for the autoregressive slots and global variable. The lack of a canonical object order to use for autoregressive inference makes learning correlations between objects fundamentally difficult. We address this by casting slot inference as a set-to-sequence modeling problem with learned object order (Figure 2 and see Algorithm 2 in the appendix). In the first stage of inference, which we describe in this section, we estimate a randomly ordered slot posterior over *segregations* of the given observation, compute order-invariant *relations* between the slots, and finally summarize relation-aware slots in a slot-order-invariant global posterior. In the second stage of inference we transform the segregation posterior into an autoregressive posterior by imposing a learned object order (Section 3.2.1) and then updating the slot posterior parameters to introduce correlations. Aligning the autoregressive slots to a learned, fixed object order helps the k^{th} autoregressive distribution learn correlations between the k^{th} slot and the previous $k - 1$ slots.

Segregate: The segregation posterior is $q_\psi(\mathbf{z}_{o_{1:K}} | \mathbf{x}) = \prod_{k=1}^K q_\psi(\mathbf{z}_{o_k} | \mathbf{x})$ with random order $o_{1:K}$. This posterior treats slots as independent. We can use any existing method to infer this posterior (e.g., GENv2 or EMORL—non-exhaustive list, details can be found in the respective papers).

Relate: We use methods from set representation learning [69; 80] to compute relations between slots in the set $\mathbf{z}_{o_{1:K}}$ and to encode this set in the scene posterior $q_\phi(\mathbf{s} | \mathbf{x})$. This posterior summarizes the

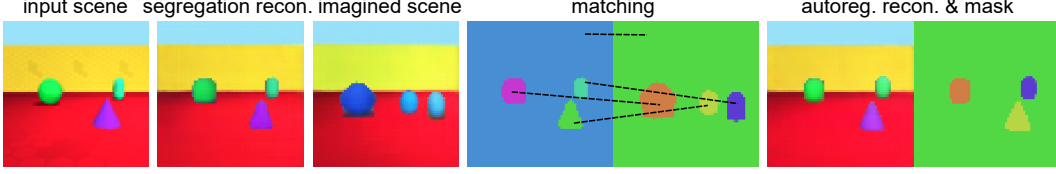


Figure 3: Imagined scenes are trained to closely resemble the input scene. This allows a meaningful matching between the randomly ordered and imagined slots to be computed (slot number indicated by mask color). The matching extracts the fixed object generation order for autoregressive inference.

object correlations in \mathbf{x} . We factorize $q_\phi(\mathbf{s} \mid \mathbf{x})$ as a product of two simpler distributions:

$$q_\phi(\mathbf{s} \mid \mathbf{x}) = \int q_\phi(\mathbf{s} \mid \underbrace{f_\phi(\mathbf{z}_{o_{1:K}})}_{\text{Relate}}) \underbrace{q_\psi(\mathbf{z}_{o_{1:K}} \mid \mathbf{x})}_{\text{Segregate}} d\mathbf{z}_{o_{1:K}}. \quad (4)$$

We use a single sample $\mathbf{z}_{o_{1:K}}$ to approximate this integral. To compute $q_\phi(\mathbf{s} \mid f_\phi(\mathbf{z}_{o_{1:K}}))$, we use a permutation-invariant neural network f_ϕ to obtain a relational embedding for $\mathbf{z}_{o_{1:K}}$. From this embedding, we compute the posterior mean and variance with two linear layers.

There are many ways to implement f_ϕ . We choose to process the slots with L set embedding layers followed by a permutation-invariant DeepSets [80] MLP with sum pooling. Each set embedding layer is implemented as residual set self-attention [69] without positional encoding:

$$\alpha = \text{softmax}\left(\frac{(\mathbf{z}_{o_{1:K}} \mathbf{W}_k)(\mathbf{z}_{o_{1:K}} \mathbf{W}_q)^\top}{\sqrt{z}}\right), \quad \hat{\mathbf{z}}_{o_i} = \sum_{j=1}^K \alpha_{ij} (\mathbf{W}_v^\top [\mathbf{z}_{o_j}; \mathbf{z}_{o_i} - \mathbf{z}_{o_j}]), \quad (5)$$

$$\mathbf{z}'_{o_i} = \mathbf{z}_{o_i} + g_\phi(\mathbf{z}_{o_i}, \mathbf{z}_{o_{1:K}}), \quad g_\phi(\mathbf{z}_{o_i}, \mathbf{z}_{o_{1:K}}) := \text{MLP}(\text{LayerNorm}(\mathbf{z}_{o_i} + \hat{\mathbf{z}}_{o_{1:K}})). \quad (6)$$

Here, $\mathbf{W}_q, \mathbf{W}_k \in \mathbb{R}^{z \times z}$, $\mathbf{W}_v \in \mathbb{R}^{2z \times z}$, $[\cdot]$ is concatenation, and α is the $K \times K$ scaled dot-product self-attention computed with keys and queries given by linear projections of $\mathbf{z}_{o_{1:K}}$. Each layer of g_ϕ shares weights across slots to preserve permutation invariance. To potentially create a stronger inductive bias for encoding directed dependencies, we explore using the difference between slots $\mathbf{z}_{o_i} - \mathbf{z}_{o_j}$ as an additional feature in Eq. 5 [61].

3.2.1 Imagining a Good Slot Order

At this point, we have inferred a segregation posterior $q_\psi(\mathbf{z}_{o_{1:K}} \mid \mathbf{x})$ and global posterior $q_\phi(\mathbf{s} \mid \mathbf{x})$. We now describe how we obtain a slot order to transform the segregation posterior into the desired autoregressive slot posterior.

Our idea to obtain a good order is to extract it from the slot prior, which we train to generate objects following a fixed order. A prior imagination rollout gives us a sequence of slots in order $\pi_{1:K}$; we extract the object order by solving a matching problem between the randomly ordered and imagined slots. Intuitively, if the imagined observation is sufficiently similar to \mathbf{x} , the imagined order should be one (of possibly many) good orders for inference on \mathbf{x} (Figure 3). The imagination rollout is:

$$\mathbf{s} \sim q_\phi(\mathbf{s} \mid \mathbf{x}), \quad \mathbf{z}_{\pi_1}, \dots, \mathbf{z}_{\pi_K} \sim p_\theta(\mathbf{z}_{\pi_1} \mid \mathbf{s}), \dots, p_\theta(\mathbf{z}_{\pi_K} \mid \mathbf{z}_{\pi_{1:K-1}}, \mathbf{s}). \quad (7)$$

In Section 3.3, we introduce an auxiliary loss to train the slot prior to learn a fixed object generation order. Extracting the order from the imagination rollout is done with an $O(K)$ greedy matching algorithm (Algorithm 1 in the appendix) that sequentially finds the best match for each slot in the rollout. Since a perfect alignment between the two sets is not guaranteed, we use $\hat{\pi}_{1:K}$ to represent the order obtained by permuting $o_{1:K}$ based on the matching. We impose $\hat{\pi}_{1:K}$ on the randomly ordered posterior by permuting the posterior means, $\mu_{o_{1:K}} \rightarrow \mu_{\hat{\pi}_{1:K}}$, and predicting new correlated variances $\bar{\sigma}_{\hat{\pi}_{1:K}}^2$ based on the order. The variances are a function of the (projected) global variable $\mathbf{W}_s^\top \mathbf{s}$ and $\mu_{\hat{\pi}_{1:K-1}}$:

$$\bar{\sigma}_{\hat{\pi}_{1:K}}^2 = \text{LSTM}([\mathbf{W}_s^\top \mathbf{s}, \mu_{\hat{\pi}_1}, \dots, \mu_{\hat{\pi}_{K-1}}]). \quad (8)$$

We do not update the permuted segregation posterior means $\mu_{\hat{\pi}_{1:K}}$ and only correlate the variances, which we find sufficient. The scene-conditional autoregressive slot posterior is

$$q_\phi(\mathbf{z}_{\hat{\pi}_{1:K}} \mid \mathbf{s}, \mathbf{x}) = q_\phi(\mathbf{z}_{\hat{\pi}_1} \mid \mathbf{s}, \mathbf{x}) \prod_{k=2}^K q_\phi(\mathbf{z}_{\hat{\pi}_k} \mid \mathbf{z}_{\hat{\pi}_{1:k-1}}, \mathbf{s}, \mathbf{x}) := \prod_{k=1}^K \mathcal{N}(\mu_{\hat{\pi}_k}, \bar{\sigma}_{\hat{\pi}_k}^2). \quad (9)$$

To ensure that the segregation VAE is not biased by ordered gradients, we prevent gradients from flowing back through $\mu_{o_{1:K}}$ and $\mathbf{z}_{o_{1:K}}$.

3.3 Training

We present SRI’s negative ELBO objective as the sum of four terms here (see the appendix for its derivation). First, we have a negative log-likelihood (reconstruction error) term:

$$\mathcal{L}_{\text{NLL}} = -\mathbb{E}_{q_\phi(\mathbf{s}|\mathbf{x})} \left[\mathbb{E}_{q_\phi(\mathbf{z}_{\hat{\pi}_{1:K}}|\mathbf{s},\mathbf{x})} [\log p_\theta(\mathbf{x} | \mathbf{z}_{\hat{\pi}_{1:K}})] \right]. \quad (10)$$

Next is a scene-level reverse Kullback-Leibler (KL) divergence term:

$$\mathcal{L}_{\text{sceneKL}} = D_{KL}(q_\phi(\mathbf{s} | \mathbf{x}) \| p(\mathbf{s})). \quad (11)$$

The slot-level reverse KL term is:

$$\begin{aligned} \mathcal{L}_{\text{slotKL}} = & \mathbb{E}_{q_\phi(\mathbf{s}|\mathbf{x})} \left[D_{KL}(q_\phi(\mathbf{z}_{\hat{\pi}_1} | \mathbf{s}, \mathbf{x}) \| p_\theta(\mathbf{z}_{\hat{\pi}_1} | \mathbf{s})) \right] \\ & + \mathbb{E}_{q_\phi(\mathbf{s}|\mathbf{x})} \left[\sum_{k=2}^K \mathbb{E}_{q_\phi(\mathbf{z}_{\hat{\pi}_{1:k-1}}|\mathbf{s},\mathbf{x})} \left[D_{KL}(q_\phi(\mathbf{z}_{\hat{\pi}_k} | \mathbf{z}_{\hat{\pi}_{1:k-1}}, \mathbf{s}, \mathbf{x}) \| p_\theta(\mathbf{z}_{\hat{\pi}_k} | \mathbf{z}_{\hat{\pi}_{1:k-1}}, \mathbf{s})) \right] \right]. \end{aligned} \quad (12)$$

Auxiliary loss: We introduce a cross-order KL term between the imagination rollout with order $\pi_{1:K}$ and autoregressive posterior with order $\hat{\pi}_{1:K}$:

$$\begin{aligned} \mathcal{L}_{\text{rolloutKL}} = & \mathbb{E}_{q_\phi(\mathbf{s}|\mathbf{x})} \left[D_{KL}(q_\phi(\mathbf{z}_{\hat{\pi}_1} | \mathbf{s}, \mathbf{x}) \| p_\theta(\mathbf{z}_{\pi_1} | \mathbf{s})) \right] \\ & + \mathbb{E}_{q_\phi(\mathbf{s}|\mathbf{x})} \left[\sum_{k=2}^K \mathbb{E}_{q_\phi(\mathbf{z}_{\hat{\pi}_{1:k-1}}|\mathbf{s},\mathbf{x})} \left[\mathbb{E}_{p_\theta(\mathbf{z}_{\pi_{1:k-1}}|\mathbf{s})} \left[D_{KL} \left(\underbrace{q_\phi(\mathbf{z}_{\hat{\pi}_k} | \star)}_{\text{Order } \hat{\pi}_{1:K}} \| \underbrace{p_\theta(\mathbf{z}_{\pi_k} | \star)}_{\text{Order } \pi_{1:K}} \right) \right] \right] \right], \end{aligned} \quad (13)$$

where $q_\phi(\mathbf{z}_{\hat{\pi}_k} | \star) := q_\phi(\mathbf{z}_{\hat{\pi}_k} | \mathbf{z}_{\hat{\pi}_{1:k-1}}, \mathbf{s}, \mathbf{x})$ and $p_\theta(\mathbf{z}_{\pi_k} | \star) := p_\theta(\mathbf{z}_{\pi_k} | \mathbf{z}_{\pi_{1:k-1}}, \mathbf{s})$. By pushing the rollout distribution towards the posterior (which is obtained from a transformation of the segregation posterior), the rollout distribution learns to adopt a fixed object order and to generate high-quality scenes (Figure 3). This loss also trains f_ϕ to extract relations from $\mathbf{z}_{o_{1:K}}$; intuitively, if the imagined observation resembles the input \mathbf{x} , then the global posterior—which we use to condition the imagination rollout—must accurately summarize correlations between $\mathbf{z}_{o_{1:K}}$.

Summary: We minimize \mathcal{L} , the sum of the objectives for the segregation VAE (\mathcal{L}_{seg}) and SRI:

$$\mathcal{L}_{\text{SRI}} = \mathcal{L}_{\text{NLL}} + \mathcal{L}_{\text{sceneKL}} + \mathcal{L}_{\text{slotKL}} + \mathcal{L}_{\text{rolloutKL}} \quad (14)$$

$$\mathcal{L} = \mathcal{L}_{\text{seg}} + \mathcal{L}_{\text{SRI}}. \quad (15)$$

We directly use the objective \mathcal{L}_{seg} as defined by the chosen segregation VAE. Similar to previous models [14; 16] we dynamically balance the reconstruction and KL terms with GECO [58]. For simplicity, we use the same SBD decoder for \mathcal{L}_{seg} and \mathcal{L}_{SRI} .

4 Experiments

In this section we analyze SRI in terms of generation quality and ability to learn correlations. Section 4.1 qualitatively evaluates random sample quality and the slot order, and Section 4.2 quantitatively compares against key baselines. We conduct ablation studies in Section 4.3. In the supplementary material we also provide videos of random walks in the learned global latent space.¹

Datasets: We use three synthetic multi-object datasets to evaluate SRI: *Objects Room* and *CLEVR6* from the standard Multi-Object Dataset [34] and *ShapeStacks* [23]. All three datasets consist of rendered images of 3D scenes containing 2-6 objects and have variable illumination, shadow, and camera perspectives. Generating scenes from these datasets requires reasoning about non-trivial correlations between objects (e.g., occlusion in CLEVR6, objects resting on the floor in Objects Room, block towers in ShapeStacks).

Setup: On all datasets we train SRI with GENv2 as the segregation VAE using both Gaussian (SRI-G) and Mixture-of-Gaussians (SRI-MoG) likelihoods. We fix $|\mathbf{z}_k| = 64$, $|\mathbf{s}| = 128$, and $L = 3$ across

¹Code and videos are available at <https://github.com/pemami4911/segregate-relate-imagine>

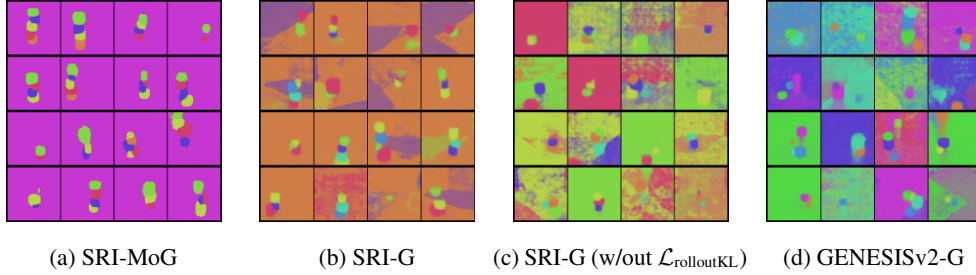


Figure 4: **Object generation order.** Slot number indicated by mask color (legend provided: Figure 6). Best viewed in color. We visualize masks for randomly generated ShapeStacks scenes. a) SRI learns to generate objects in a fixed order. For this training run, the model uses slot 1 for the background and slots 4-9 for blocks (most towers have only 2-4 blocks). b) SRI-G uses slots 1 and 5 for background and 6-9 for blocks (occasionally 3-4). c) Without the cross-order KL term, SRI’s prior does not learn a fixed order and instead we see it uses random permutations of slots 5-9. d) GENv2-G fails to learn a fixed order which hinders learning correlations.

environments. Following standard practice, on CLEVR6 and Objects Room we use $K = 7$ and on ShapeStacks we use $K = 9$.

Baselines: We compare against the state-of-the-art slot VAEs for scene generation GEN and GENv2, as well as EMORL and GNM (not slot-based). Results for GEN and GENv2 (GENv2-MoG) are taken from Engelcke et al. [16] (both use the Mixture-of-Gaussians by default). GEN and GENv2-MoG results were missing for CLEVR6 so we trained these ourselves with the official code releases. We also train GENv2 with the Gaussian likelihood (GENv2-G) on all three datasets to provide a direct comparison for SRI-G. GNM and EMORL are trained on all datasets using official code releases. Remaining architecture, hyperparameters, and compute details can be found in the appendix.

4.1 Qualitative Evaluation

First, we visualize segmentation masks for randomly generated ShapeStacks scenes which show that SRI learns a fixed generation order (Figure 4). We also show that GENv2 fails to learn a fixed order which hurts its ability to learn object correlations (Figure 4d). Then, we compare random scenes sampled from each generative model in Figure 5 with addition samples from SRI in the appendix (Figures 7, 8). Across environments, SRI generates the highest quality scenes. GENv2’s samples contain artifacts and structural inaccuracies (e.g., extra walls and missing floors in Objects Room for GENv2-G and floating blocks in ShapeStacks). Specifically, on Objects Room GENv2-MoG tends to segregate the walls, floor, and sky into a single slot while GENv2-G segments the background across multiple slots. This increases the difficulty of learning multi-object correlations for GENv2-G, which SRI-G addresses. GEN’s sequential attention occasionally settles on a semi-consistent order (e.g., placing the background in the first slot for CLEVR6 and Objects Room) but in general this order is arbitrary and its attention mechanism fails on challenging scenes. As expected due to its independent slot prior, EMORL generates incoherent scenes. GNM generates images of high quality yet does so at the expense of poor segmentation quality. It is particularly challenged by Objects Room and ShapeStacks due to object occlusion and variable object sizes. See Appendix A.5 for extra random samples, test time generation with different numbers of slots K , imagination rollouts, and more.

4.2 Quantitative Evaluation

We use the Fréchet Inception Distance (FID) [27] to quantify the visual similarity of generated scenes to training scenes. Inspired by the evaluation in GNM [32], we measure the ability to learn higher-order correlations by manually labeling 100 ShapeStacks scenes generated by each model and computing the percent of scenes that contain a physically plausible stack of blocks, i.e., all blocks in the stack are touching each other (structural accuracy, or **S-Acc**). We use officially released model weights to compute S-Acc for GEN and GENv2-MoG. We follow standard practice for evaluating segregation quality, which is to use the adjusted rand index [57; 29] for foreground objects only with ground truth masks (**ARI-FG**).

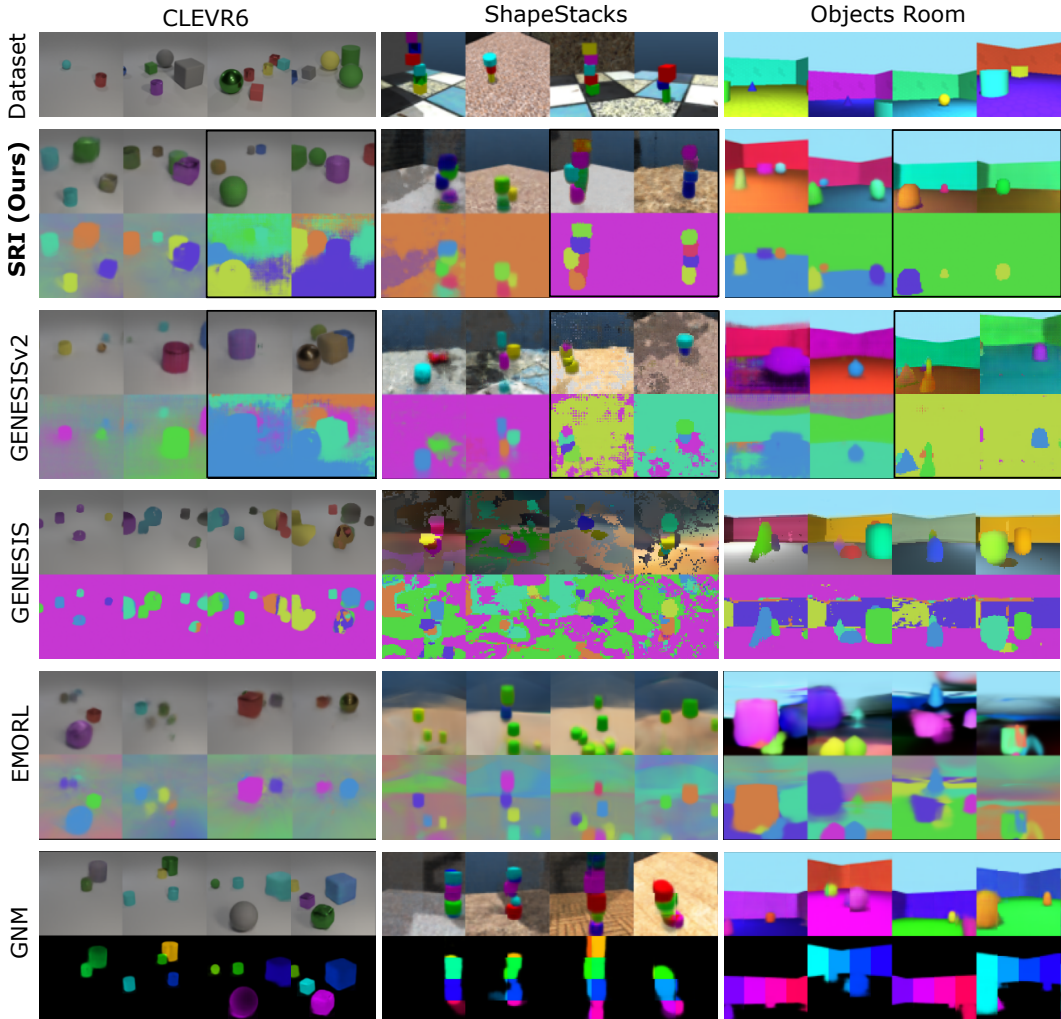


Figure 5: **Randomly generated scenes.** Samples from SRI-MoG and GENv2-MoG are outlined in black. SRI generates scenes (both images and object masks) of the highest quality and that best reflect correlations present in the training data. Best viewed zoomed in and in color.

Results are in Table 1. Out of the slot VAEs, SRI achieves the lowest FID scores on all environments and the best S-Acc score. SRI-G improves GENv2-G’s FID by an average of 24% and SRI-MoG improves GENv2-MoG’s FID by an average of 19%. On CLEVR6, we observe that SRI achieves the smallest improvement in FID over GENv2, which we believe is caused by *i)* CLEVR6 only having simple correlations to learn (e.g., occlusion) and *ii)* small artifacts introduced by GENv2’s encoder which seems to negatively impact the FID score on this dataset. To check this, and to demonstrate the flexibility of SRI, we also train SRI with EMORL as the segregation VAE on CLEVR6. We see a significant improvement in FID from EMORL to SRI-EMORL (244 ± 19 to 48.9 ± 7 , also see Figure 12). GENv2-G segregates the walls, floor, and sky into different slots on Objects Room which makes correlation learning difficult, leading to a poor FID score and which SRI-G improves by 36%. In general, we find that the segregation quality of SRI closely matches that of the slot VAE used for scene segregation, and that better ARI-FG correlates with better sample quality for SRI. GNM’s difficulty with segregating Objects Room and ShapeStacks scenes is reflected by its comparatively low ARI-FG scores on two out of three environments.

4.3 Ablation Study

On ShapeStacks’s validation set we carefully ablate the core aspects of SRI (Table 2). *a)* Removing the global variable and instead using a slot prior with $p(\mathbf{z}_1) := \mathcal{N}(0, 1)$ significantly hurts sample

Table 1: **Main quantitative results.** Mean \pm std. dev. over 3 training runs. Results* are from Engelcke et al. [16]. Best generation results for slot VAEs are in bold.

Model	Slot VAE	CLEVR6		Objects Room		ShapeStacks		
		FID \downarrow	ARI-FG \uparrow	FID \downarrow	ARI-FG \uparrow	FID \downarrow	ARI-FG \uparrow	S-Acc (%) \uparrow
GNM	\times	27.5 \pm 1	0.97 \pm 0.01	51.6 \pm 5	0.63 \pm 0.00	49.3 \pm 2	0.37 \pm 0.07	100.0 \pm 0.0
GEN	\checkmark	116.9 \pm 4	0.82 \pm 0.07	62.8* \pm 3	0.63* \pm 0.03	186.8* \pm 18	0.70* \pm 0.05	0
EMORL	\checkmark	244.0 \pm 19	0.96 \pm 0.02	178.3 \pm 27	0.47 \pm 0.22	258.4 \pm 57	0.60 \pm 0.04	0
GENv2-G	\checkmark	61.0 \pm 3	0.98 \pm 0.00	87.6 \pm 4	0.75 \pm 0.02	115.3 \pm 6	0.68 \pm 0.02	50.7 \pm 3.1
GENv2-MoG	\checkmark	61.0 \pm 3	0.98 \pm 0.00	52.6* \pm 3	0.84* \pm 0.01	112.7* \pm 3	0.81* \pm 0.00	59
SRI-G	\checkmark	60.6 \pm 8	0.96 \pm 0.02	55.7 \pm 4	0.74 \pm 0.01	74.7 \pm 5	0.70 \pm 0.01	72.0 \pm 3.5
SRI-MoG	\checkmark	54.4 \pm 2	0.97 \pm 0.01	48.4 \pm 4	0.83 \pm 0.02	70.4 \pm 3	0.78 \pm 0.02	80.7 \pm 5.0

Table 2: **Ablations with SRI-G on ShapeStacks.** Mean \pm std. dev. over 3 runs. The negative ELBO in bits-per-dim (bpd) is a single sample Monte Carlo estimate averaged over 5k validation scenes.

	Learned order	Global variable	$\mathcal{L}_{\text{rolloutKL}}$	Attention	FID \downarrow	$\mathcal{L}_{\text{SRI}}(\text{bpd})\downarrow$	S-Acc (%) \uparrow	
a)	\checkmark		\checkmark	-	132.9 \pm 2	(-57.9)	0.836 \pm 0.001	31.7 \pm 6.4
b)		\checkmark	-	\checkmark	123.2 \pm 3	(-48.2)	0.845 \pm 0.001	43.7 \pm 10.7
c)	\checkmark	\checkmark		\checkmark	106.3 \pm 3	(-31.3)	0.833 \pm 0.001	61.3 \pm 1.5
d)	\checkmark	\checkmark	\checkmark		77.4 \pm 2	(-2.4)	0.829 \pm 0.000	72.0 \pm 3.6
e)	\checkmark	\checkmark	\checkmark	\checkmark	75.0 \pm 6	(+0.0)	0.829 \pm 0.001	72.0 \pm 3.5

quality. Without the global variable, higher-order correlations are difficult to learn and the imagination rollout is *unconditional* meaning it is unrelated to the input \mathbf{x} . As a result SRI fails to learn a fixed generation order. *b)* Here, we do not try to align the slot order for inference and instead train the autoregressive slot posterior using the random order $o_{1:K}$ (therefore also removing $\mathcal{L}_{\text{rolloutKL}}$ from the loss). SRI struggles to learn object correlations and sample quality is also poor. *c)* If we remove $\mathcal{L}_{\text{rolloutKL}}$ from the loss, SRI’s prior fails to learn a fixed order and correlation estimation suffers. This results in a significant drop in sample quality (see Figure 4c). *d)* We remove the relational attention by dropping $\hat{\mathbf{z}}_{o_{1:K}}$ from Eq. 6. This incurs only a small increase in FID, likely because the DeepSets MLP is reasonably expressive for learning correlations and because other aspects such as segregation quality seem to have a larger impact on FID. In general, we see that *the global variable, learned order, and cross-order KL loss all play a critical role in SRI.*

5 Conclusion

In this work we demonstrated that slot order matters for compositional scene understanding because it facilitates learning complex multi-object correlations. We contributed SRI, a hierarchical VAE with autoregressive slots and a global scene-level prior. Inference is cast as a set-to-sequence problem which allows us to learn a good object order for autoregressive inference. Our empirical results demonstrate that SRI significantly improves the sample quality of compositionally generated scenes for slot VAEs. Moreover, with SRI, future advances that improve our ability to segregate scenes should now directly translate to better sample quality.

One limitation of SRI is the lack of 3D reasoning. Although unsupervised 3D reasoning is challenging due to the ambiguities introduced by perspective geometry [7; 65; 76; 19], a 3D understanding of objects should further improve generation quality. Another limitation is that SRI does not learn causal dependencies between objects but rather only correlations, which only weakly generalize outside the training distribution [62]. Extending SRI to dynamic settings would enable exploring causal inference of dependencies. Finally, we suspect that the standard Gaussian global prior we used for simplicity is sub-optimal for learning higher-order correlations. Exploring more flexible global priors could further improve results.

While there are not immediate negative societal implications of this work, future work that builds on our ideas could be applied to realistic data which could plausibly cause harm. Generative models capable of synthesizing photo-realistic scenes could be used, for example, as part of a disinformation campaign. Research on mitigation strategies for such scenarios is ongoing [49].

Acknowledgements

We thank Dave Biagioni and Peter Graf for providing valuable comments and suggested revisions. Patrick Emami was supported in parts by the Florida DOT under grant BDV31 977-116, an FEF McKnight fellowship, and the National Renewable Energy Laboratory, operated by Alliance for Sustainable Energy, LLC, for the U.S. Department of Energy (DOE) under Contract No. DE-AC36-08GO28308. This work was supported by the Laboratory Directed Research and Development (LDRD) Program at NREL. The views expressed in the article do not necessarily represent the views of the DOE or the U.S. Government. The U.S. Government retains and the publisher, by accepting the article for publication, acknowledges that the U.S. Government retains a nonexclusive, paid-up, irrevocable, worldwide license to publish or reproduce the published form of this work, or allow others to do so, for U.S. Government purposes.

References

- [1] Adams, R. P. and Zemel, R. S. Ranking via sinkhorn propagation. *ArXiv preprint*, abs/1106.1925, 2011. URL <https://arxiv.org/abs/1106.1925>.
- [2] Anciukevicius, T., Lampert, C. H., and Henderson, P. Object-centric image generation with factored depths, locations, and appearances. *ArXiv preprint*, abs/2004.00642, 2020. URL <https://arxiv.org/abs/2004.00642>.
- [3] Arad Hudson, D. and Zitnick, L. Compositional transformers for scene generation. *Advances in Neural Information Processing Systems*, 34, 2021.
- [4] Baillargeon, R. Infants’ physical world. *Current directions in psychological science*, 13(3): 89–94, 2004.
- [5] Battaglia, P. W., Hamrick, J. B., and Tenenbaum, J. B. Simulation as an engine of physical scene understanding. *Proceedings of the National Academy of Sciences*, 110(45):18327–18332, 2013.
- [6] Burgess, C. P., Matthey, L., Watters, N., Kabra, R., Higgins, I., Botvinick, M., and Lerchner, A. MONet: Unsupervised scene decomposition and representation. *ArXiv preprint*, abs/1901.11390, 2019. URL <https://arxiv.org/abs/1901.11390>.
- [7] Chen, C., Deng, F., and Ahn, S. Roots: Object-centric representation and rendering of 3d scenes. *Journal of Machine Learning Research*, 22(259):1–36, 2021.
- [8] Chen, M., Radford, A., Child, R., Wu, J., Jun, H., Luan, D., and Sutskever, I. Generative pretraining from pixels. In *Proceedings of the 37th International Conference on Machine Learning, ICML 2020, 13-18 July 2020, Virtual Event*, volume 119 of *Proceedings of Machine Learning Research*, pp. 1691–1703. PMLR, 2020. URL <http://proceedings.mlr.press/v119/chen20s.html>.
- [9] Child, R., Gray, S., Radford, A., and Sutskever, I. Generating long sequences with sparse transformers. *ArXiv preprint*, abs/1904.10509, 2019. URL <https://arxiv.org/abs/1904.10509>.
- [10] Crawford, E. and Pineau, J. Spatially invariant unsupervised object detection with convolutional neural networks. In *The Thirty-Third AAAI Conference on Artificial Intelligence, AAAI 2019, The Thirty-First Innovative Applications of Artificial Intelligence Conference, IAAI 2019, The Ninth AAAI Symposium on Educational Advances in Artificial Intelligence, EAAI 2019, Honolulu, Hawaii, USA, January 27 - February 1, 2019*, pp. 3412–3420. AAAI Press, 2019. doi: 10.1609/aaai.v33i01.33013412. URL <https://doi.org/10.1609/aaai.v33i01.33013412>.
- [11] Creswell, A., Kabra, R., Burgess, C., and Shanahan, M. Unsupervised object-based transition models for 3d partially observable environments. *Advances in Neural Information Processing Systems*, 34, 2021.
- [12] Deng, F., Zhi, Z., Lee, D., and Ahn, S. Generative scene graph networks. In *9th International Conference on Learning Representations, ICLR 2021, Virtual Event, Austria, May 3-7, 2021*. OpenReview.net, 2021. URL <https://openreview.net/forum?id=RmcPm9m3tnk>.

- [13] Ehrhardt, S., Groth, O., Monzpart, A., Engelcke, M., Posner, I., Mitra, N. J., and Vedaldi, A. RELATE: physically plausible multi-object scene synthesis using structured latent spaces. In Larochelle, H., Ranzato, M., Hadsell, R., Balcan, M., and Lin, H. (eds.), *Advances in Neural Information Processing Systems 33: Annual Conference on Neural Information Processing Systems 2020, NeurIPS 2020, December 6-12, 2020, virtual*, 2020. URL <https://proceedings.neurips.cc/paper/2020/hash/806beafe154032a5b818e97b4420ad98-Abstract.html>.
- [14] Emami, P., He, P., Ranka, S., and Rangarajan, A. Efficient iterative amortized inference for learning symmetric and disentangled multi-object representations. In Meila, M. and Zhang, T. (eds.), *Proceedings of the 38th International Conference on Machine Learning, ICML 2021, 18-24 July 2021, Virtual Event*, volume 139 of *Proceedings of Machine Learning Research*, pp. 2970–2981. PMLR, 2021. URL <http://proceedings.mlr.press/v139/emami21a.html>.
- [15] Engelcke, M., Kosiorek, A. R., Jones, O. P., and Posner, I. GENESIS: generative scene inference and sampling with object-centric latent representations. In *8th International Conference on Learning Representations, ICLR 2020, Addis Ababa, Ethiopia, April 26-30, 2020*. OpenReview.net, 2020. URL <https://openreview.net/forum?id=BkxfaTVFwH>.
- [16] Engelcke, M., Parker Jones, O., and Posner, I. GENESIS-V2: Inferring unordered object representations without iterative refinement. In Ranzato, M., Beygelzimer, A., Dauphin, Y., Liang, P., and Vaughan, J. W. (eds.), *Advances in Neural Information Processing Systems*, volume 34, pp. 8085–8094. Curran Associates, Inc., 2021. URL <https://proceedings.neurips.cc/paper/2021/file/43ec517d68b6edd3015b3edc9a11367b-Paper.pdf>.
- [17] Eslami, S. M. A., Heess, N., Weber, T., Tassa, Y., Szepesvari, D., Kavukcuoglu, K., and Hinton, G. E. Attend, infer, repeat: Fast scene understanding with generative models. In Lee, D. D., Sugiyama, M., von Luxburg, U., Guyon, I., and Garnett, R. (eds.), *Advances in Neural Information Processing Systems 29: Annual Conference on Neural Information Processing Systems 2016, December 5-10, 2016, Barcelona, Spain*, pp. 3225–3233, 2016. URL <https://proceedings.neurips.cc/paper/2016/hash/52947e0ade57a09e4a1386d08f17b656-Abstract.html>.
- [18] Glorot, X. and Bengio, Y. Understanding the difficulty of training deep feedforward neural networks. In *Proceedings of the thirteenth international conference on artificial intelligence and statistics*, pp. 249–256. JMLR Workshop and Conference Proceedings, 2010.
- [19] Gothoskar, N., Cusumano-Towner, M., Zinberg, B., Ghavamizadeh, M., Pollok, F., Garrett, A., Tenenbaum, J., Gutfreund, D., and Mansinghka, V. 3DP3: 3d scene perception via probabilistic programming. *Advances in Neural Information Processing Systems*, 34, 2021.
- [20] Greff, K., Klein, A., Chovanec, M., Hutter, F., and Schmidhuber, J. The sacred infrastructure for computational research. In *Proceedings of the 15th python in science conference (SciPy 2017)*, volume 28, pp. 49–56, 2017.
- [21] Greff, K., Kaufman, R. L., Kabra, R., Watters, N., Burgess, C., Zoran, D., Matthey, L., Botvinick, M., and Lerchner, A. Multi-object representation learning with iterative variational inference. In Chaudhuri, K. and Salakhutdinov, R. (eds.), *Proceedings of the 36th International Conference on Machine Learning, ICML 2019, 9-15 June 2019, Long Beach, California, USA*, volume 97 of *Proceedings of Machine Learning Research*, pp. 2424–2433. PMLR, 2019. URL <http://proceedings.mlr.press/v97/greff19a.html>.
- [22] Greff, K., van Steenkiste, S., and Schmidhuber, J. On the binding problem in artificial neural networks. *ArXiv preprint*, abs/2012.05208, 2020. URL <https://arxiv.org/abs/2012.05208>.
- [23] Groth, O., Fuchs, F. B., Posner, I., and Vedaldi, A. Shapestacks: Learning vision-based physical intuition for generalised object stacking. In *Proceedings of the European Conference on Computer Vision (ECCV)*, pp. 702–717, 2018.
- [24] Grover, A., Wang, E., Zweig, A., and Ermon, S. Stochastic optimization of sorting networks via continuous relaxations. In *7th International Conference on Learning Representations, ICLR 2019, New Orleans, LA, USA, May 6-9, 2019*. OpenReview.net, 2019. URL <https://openreview.net/forum?id=H1eSS3CckX>.

- [25] Harris, C. R., Millman, K. J., van der Walt, S. J., Gommers, R., Virtanen, P., Cournapeau, D., Wieser, E., Taylor, J., Berg, S., Smith, N. J., Kern, R., Picus, M., Hoyer, S., van Kerkwijk, M. H., Brett, M., Haldane, A., del Río, J. F., Wiebe, M., Peterson, P., Gérard-Marchant, P., Sheppard, K., Reddy, T., Weckesser, W., Abbasi, H., Gohlke, C., and Oliphant, T. E. Array programming with NumPy. *Nature*, 585(7825):357–362, 2020. ISSN 1476-4687. doi: 10.1038/s41586-020-2649-2. URL <https://doi.org/10.1038/s41586-020-2649-2>.
- [26] Hendrycks, D. and Gimpel, K. Gaussian error linear units (gelus). *ArXiv preprint*, abs/1606.08415, 2016. URL <https://arxiv.org/abs/1606.08415>.
- [27] Heusel, M., Ramsauer, H., Unterthiner, T., Nessler, B., and Hochreiter, S. GANs trained by a two time-scale update rule converge to a local nash equilibrium. In Guyon, I., von Luxburg, U., Bengio, S., Wallach, H. M., Fergus, R., Vishwanathan, S. V. N., and Garnett, R. (eds.), *Advances in Neural Information Processing Systems 30: Annual Conference on Neural Information Processing Systems 2017, December 4-9, 2017, Long Beach, CA, USA*, pp. 6626–6637, 2017. URL <https://proceedings.neurips.cc/paper/2017/hash/8a1d694707eb0fefe65871369074926d-Abstract.html>.
- [28] Hochreiter, S. and Schmidhuber, J. Long short-term memory. *Neural computation*, 9(8): 1735–1780, 1997.
- [29] Hubert, L. and Arabie, P. Comparing partitions. *Journal of classification*, 2(1):193–218, 1985.
- [30] Hudson, D. A. and Zitnick, L. Generative adversarial transformers. In Meila, M. and Zhang, T. (eds.), *Proceedings of the 38th International Conference on Machine Learning, ICML 2021, 18-24 July 2021, Virtual Event*, volume 139 of *Proceedings of Machine Learning Research*, pp. 4487–4499. PMLR, 2021. URL <http://proceedings.mlr.press/v139/hudson21a.html>.
- [31] Hunter, J. D. Matplotlib: A 2D Graphics Environment. *Computing in Science & Engineering*, 9(3):90–95, 2007.
- [32] Jiang, J. and Ahn, S. Generative neurosymbolic machines. In Larochelle, H., Ranzato, M., Hadsell, R., Balcan, M., and Lin, H. (eds.), *Advances in Neural Information Processing Systems 33: Annual Conference on Neural Information Processing Systems 2020, NeurIPS 2020, December 6-12, 2020, virtual*, 2020. URL <https://proceedings.neurips.cc/paper/2020/hash/94c28dcfc97557df0df6d1f7222fc384-Abstract.html>.
- [33] Jurewicz, M. and Derczynski, L. Set-to-sequence methods in machine learning: a review. *Journal of Artificial Intelligence Research*, 71:885–924, 2021.
- [34] Kabra, R., Burgess, C., Matthey, L., Kaufman, R. L., Greff, K., Reynolds, M., and Lerchner, A. Multi-object datasets, 2019. URL <https://github.com/deepmind/multi-object-datasets/>.
- [35] Kabra, R., Zoran, D., Erdogan, G., Matthey, L., Creswell, A., Botvinick, M., Lerchner, A., and Burgess, C. SIMONE: View-invariant, temporally-abstracted object representations via unsupervised video decomposition. In Ranzato, M., Beygelzimer, A., Dauphin, Y., Liang, P., and Vaughan, J. W. (eds.), *Advances in Neural Information Processing Systems*, volume 34, pp. 20146–20159. Curran Associates, Inc., 2021. URL <https://proceedings.neurips.cc/paper/2021/file/a860a7886d7c7e2a8d3eaac96f76dc0d-Paper.pdf>.
- [36] Kahneman, D., Treisman, A., and Gibbs, B. J. The reviewing of object files: Object-specific integration of information. *Cognitive psychology*, 24(2):175–219, 1992.
- [37] Kingma, D. P. and Ba, J. Adam: A method for stochastic optimization. In Bengio, Y. and LeCun, Y. (eds.), *3rd International Conference on Learning Representations, ICLR 2015, San Diego, CA, USA, May 7-9, 2015, Conference Track Proceedings*, 2015. URL <http://arxiv.org/abs/1412.6980>.
- [38] Kingma, D. P. and Welling, M. Auto-encoding variational bayes. In Bengio, Y. and LeCun, Y. (eds.), *2nd International Conference on Learning Representations, ICLR 2014, Banff, AB, Canada, April 14-16, 2014, Conference Track Proceedings*, 2014. URL <http://arxiv.org/abs/1312.6114>.

- [39] Kluyver, T., Ragan-Kelley, B., Pérez, F., Granger, B., Bussonnier, M., Frederic, J., Kelley, K., Hamrick, J., Grout, J., Corlay, S., Ivanov, P., Avila, D., Abdalla, S., and Willing, C. Jupyter Notebooks – a publishing format for reproducible computational workflows. In Loizides, F. and Schmidt, B. (eds.), *Positioning and Power in Academic Publishing: Players, Agents and Agendas*, pp. 87 – 90. IOS Press, 2016.
- [40] Lake, B. M., Ullman, T. D., Tenenbaum, J. B., and Gershman, S. J. Building machines that learn and think like people. *Behavioral and brain sciences*, 40, 2017.
- [41] Li, N., Eastwood, C., and Fisher, R. B. Learning object-centric representations of multi-object scenes from multiple views. In Larochelle, H., Ranzato, M., Hadsell, R., Balcan, M., and Lin, H. (eds.), *Advances in Neural Information Processing Systems 33: Annual Conference on Neural Information Processing Systems 2020, NeurIPS 2020, December 6-12, 2020, virtual*, 2020. URL <https://proceedings.neurips.cc/paper/2020/hash/3d9dabe52805a1ea21864b09f3397593-Abstract.html>.
- [42] Li, N., Raza, M. A., Hu, W., Sun, Z., and Fisher, R. Object-centric representation learning with generative spatial-temporal factorization. *Advances in Neural Information Processing Systems*, 34, 2021.
- [43] Li, X., Trabucco, B., Park, D. H., Luo, M., Shen, S., Darrell, T., and Gao, Y. Discovering non-monotonic autoregressive orderings with variational inference. In *9th International Conference on Learning Representations, ICLR 2021, Virtual Event, Austria, May 3-7, 2021*. OpenReview.net, 2021. URL <https://openreview.net/forum?id=jP1vTH3inC>.
- [44] Liao, Y., Schwarz, K., Mescheder, L. M., and Geiger, A. Towards unsupervised learning of generative models for 3d controllable image synthesis. In *2020 IEEE/CVF Conference on Computer Vision and Pattern Recognition, CVPR 2020, Seattle, WA, USA, June 13-19, 2020*, pp. 5870–5879. IEEE, 2020. doi: 10.1109/CVPR42600.2020.00591. URL <https://doi.org/10.1109/CVPR42600.2020.00591>.
- [45] Lin, Z., Wu, Y., Peri, S. V., Fu, B., Jiang, J., and Ahn, S. Improving generative imagination in object-centric world models. In *Proceedings of the 37th International Conference on Machine Learning, ICML 2020, 13-18 July 2020, Virtual Event*, volume 119 of *Proceedings of Machine Learning Research*, pp. 6140–6149. PMLR, 2020. URL <http://proceedings.mlr.press/v119/lin20f.html>.
- [46] Lin, Z., Wu, Y., Peri, S. V., Sun, W., Singh, G., Deng, F., Jiang, J., and Ahn, S. SPACE: unsupervised object-oriented scene representation via spatial attention and decomposition. In *8th International Conference on Learning Representations, ICLR 2020, Addis Ababa, Ethiopia, April 26-30, 2020*. OpenReview.net, 2020. URL <https://openreview.net/forum?id=rk103ySYDH>.
- [47] Locatello, F., Weissenborn, D., Unterthiner, T., Mahendran, A., Heigold, G., Uszkoreit, J., Dosovitskiy, A., and Kipf, T. Object-centric learning with slot attention. In Larochelle, H., Ranzato, M., Hadsell, R., Balcan, M., and Lin, H. (eds.), *Advances in Neural Information Processing Systems 33: Annual Conference on Neural Information Processing Systems 2020, NeurIPS 2020, December 6-12, 2020, virtual*, 2020. URL <https://proceedings.neurips.cc/paper/2020/hash/8511df98c02ab60aea1b2356c013bc0f-Abstract.html>.
- [48] Mena, G. E., Belanger, D., Linderman, S. W., and Snoek, J. Learning latent permutations with gumbel-sinkhorn networks. In *6th International Conference on Learning Representations, ICLR 2018, Vancouver, BC, Canada, April 30 - May 3, 2018, Conference Track Proceedings*. OpenReview.net, 2018. URL <https://openreview.net/forum?id=Byt3oJ-0W>.
- [49] Mishkin, P., Ahmad, L., Brundage, M., Krueger, G., and Sastry, G. Dall-e 2 preview - risks and limitations. 2022. URL <https://github.com/openai/dalle-2-preview/blob/main/system-card.md>.
- [50] Munkres, J. Algorithms for the assignment and transportation problems. *Journal of the society for industrial and applied mathematics*, 5(1):32–38, 1957.

- [51] Nguyen-Phuoc, T., Richardt, C., Mai, L., Yang, Y., and Mitra, N. J. BlockGAN: learning 3d object-aware scene representations from unlabelled images. In Larochelle, H., Ranzato, M., Hadsell, R., Balcan, M., and Lin, H. (eds.), *Advances in Neural Information Processing Systems 33: Annual Conference on Neural Information Processing Systems 2020, NeurIPS 2020, December 6-12, 2020, virtual*, 2020. URL <https://proceedings.neurips.cc/paper/2020/hash/4b29fa4efe4fb7bc667c7b301b74d52d-Abstract.html>.
- [52] Niemeyer, M. and Geiger, A. GIRAFFE: Representing scenes as compositional generative neural feature fields. In *Proceedings of the IEEE/CVF Conference on Computer Vision and Pattern Recognition*, pp. 11453–11464, 2021.
- [53] Parmar, N., Vaswani, A., Uszkoreit, J., Kaiser, L., Shazeer, N., Ku, A., and Tran, D. Image transformer. In Dy, J. G. and Krause, A. (eds.), *Proceedings of the 35th International Conference on Machine Learning, ICML 2018, Stockholm, Sweden, July 10-15, 2018*, volume 80 of *Proceedings of Machine Learning Research*, pp. 4052–4061. PMLR, 2018. URL <http://proceedings.mlr.press/v80/parmar18a.html>.
- [54] Paszke, A., Gross, S., Massa, F., Lerer, A., Bradbury, J., Chanan, G., Killeen, T., Lin, Z., Gimelshein, N., Antiga, L., Desmaison, A., Kopf, A., Yang, E., DeVito, Z., Raison, M., Tejani, A., Chilamkurthy, S., Steiner, B., Fang, L., Bai, J., and Chintala, S. PyTorch: An Imperative Style, High-Performance Deep Learning Library. In *Advances in Neural Information Processing Systems 32*, pp. 8024–8035. Curran Associates, Inc., 2019.
- [55] Pedregosa, F., Varoquaux, G., Gramfort, A., Michel, V., Thirion, B., Grisel, O., Blondel, M., Prettenhofer, P., Weiss, R., Dubourg, V., Vanderplas, J., Passos, A., Cournapeau, D., Brucher, M., Perrot, M., and Édouard Duchesnay. Scikit-learn: Machine Learning in Python. *Journal of Machine Learning Research*, 12(85):2825–2830, 2011. URL <http://jmlr.org/papers/v12/pedregosa11a.html>.
- [56] Ramesh, A., Pavlov, M., Goh, G., Gray, S., Voss, C., Radford, A., Chen, M., and Sutskever, I. Zero-shot text-to-image generation. In Meila, M. and Zhang, T. (eds.), *Proceedings of the 38th International Conference on Machine Learning*, volume 139 of *Proceedings of Machine Learning Research*, pp. 8821–8831. PMLR, 18–24 Jul 2021. URL <https://proceedings.mlr.press/v139/ramesh21a.html>.
- [57] Rand, W. M. Objective criteria for the evaluation of clustering methods. *Journal of the American Statistical Association*, 66(336):846–850, 1971.
- [58] Rezende, D. J. and Viola, F. Taming VAEs. *ArXiv preprint*, abs/1810.00597, 2018. URL <https://arxiv.org/abs/1810.00597>.
- [59] Rezende, D. J., Mohamed, S., and Wierstra, D. Stochastic backpropagation and approximate inference in deep generative models. In *Proceedings of the 31th International Conference on Machine Learning, ICML 2014, Beijing, China, 21-26 June 2014*, volume 32 of *JMLR Workshop and Conference Proceedings*, pp. 1278–1286. JMLR.org, 2014. URL <http://proceedings.mlr.press/v32/rezende14.html>.
- [60] Salimans, T., Karpathy, A., Chen, X., and Kingma, D. P. Pixelcnn++: Improving the pixelcnn with discretized logistic mixture likelihood and other modifications. In *5th International Conference on Learning Representations, ICLR 2017, Toulon, France, April 24-26, 2017, Conference Track Proceedings*. OpenReview.net, 2017. URL <https://openreview.net/forum?id=BJrFC6ceg>.
- [61] Santoro, A., Raposo, D., Barrett, D. G. T., Malinowski, M., Pascanu, R., Battaglia, P. W., and Lillicrap, T. A simple neural network module for relational reasoning. In Guyon, I., von Luxburg, U., Bengio, S., Wallach, H. M., Fergus, R., Vishwanathan, S. V. N., and Garnett, R. (eds.), *Advances in Neural Information Processing Systems 30: Annual Conference on Neural Information Processing Systems 2017, December 4-9, 2017, Long Beach, CA, USA*, pp. 4967–4976, 2017. URL <https://proceedings.neurips.cc/paper/2017/hash/e6acf4b0f69f6f6e60e9a815938aa1ff-Abstract.html>.
- [62] Schölkopf, B., Locatello, F., Bauer, S., Ke, N. R., Kalchbrenner, N., Goyal, A., and Bengio, Y. Toward causal representation learning. *Proceedings of the IEEE*, 109(5):612–634, 2021.

- [63] Singh, G., Deng, F., and Ahn, S. Illiterate DALL-E learns to compose. In *10th International Conference on Learning Representations, ICLR 2022*, 2022.
- [64] Spelke, E. S. and Kinzler, K. D. Core knowledge. *Developmental science*, 10(1):89–96, 2007.
- [65] Stelzner, K., Kersting, K., and Kosiorek, A. R. Decomposing 3d scenes into objects via unsupervised volume segmentation. *ArXiv preprint*, abs/2104.01148, 2021. URL <https://arxiv.org/abs/2104.01148>.
- [66] Vahdat, A. and Kautz, J. NVAE: A deep hierarchical variational autoencoder. In Larochelle, H., Ranzato, M., Hadsell, R., Balcan, M., and Lin, H. (eds.), *Advances in Neural Information Processing Systems 33: Annual Conference on Neural Information Processing Systems 2020, NeurIPS 2020, December 6-12, 2020, virtual*, 2020. URL <https://proceedings.neurips.cc/paper/2020/hash/e3b21256183cf7c2c7a66be163579d37-Abstract.html>.
- [67] van den Oord, A., Kalchbrenner, N., Espeholt, L., Kavukcuoglu, K., Vinyals, O., and Graves, A. Conditional image generation with pixelcnn decoders. In Lee, D. D., Sugiyama, M., von Luxburg, U., Guyon, I., and Garnett, R. (eds.), *Advances in Neural Information Processing Systems 29: Annual Conference on Neural Information Processing Systems 2016, December 5-10, 2016, Barcelona, Spain*, pp. 4790–4798, 2016. URL <https://proceedings.neurips.cc/paper/2016/hash/b1301141feffabac455e1f90a7de2054-Abstract.html>.
- [68] van Steenkiste, S., Kurach, K., Schmidhuber, J., and Gelly, S. Investigating object compositionality in generative adversarial networks. *Neural Networks*, 130:309–325, 2020. ISSN 0893-6080. doi: <https://doi.org/10.1016/j.neunet.2020.07.007>. URL <https://www.sciencedirect.com/science/article/pii/S0893608020302483>.
- [69] Vaswani, A., Shazeer, N., Parmar, N., Uszkoreit, J., Jones, L., Gomez, A. N., Kaiser, L., and Polosukhin, I. Attention is all you need. In Guyon, I., von Luxburg, U., Bengio, S., Wallach, H. M., Fergus, R., Vishwanathan, S. V. N., and Garnett, R. (eds.), *Advances in Neural Information Processing Systems 30: Annual Conference on Neural Information Processing Systems 2017, December 4-9, 2017, Long Beach, CA, USA*, pp. 5998–6008, 2017. URL <https://proceedings.neurips.cc/paper/2017/hash/3f5ee243547dee91fbd053c1c4a845aa-Abstract.html>.
- [70] Veerapaneni, R., Co-Reyes, J. D., Chang, M., Janner, M., Finn, C., Wu, J., Tenenbaum, J. B., and Levine, S. Entity abstraction in visual model-based reinforcement learning. *ArXiv preprint*, abs/1910.12827, 2019. URL <https://arxiv.org/abs/1910.12827>.
- [71] Vinyals, O., Fortunato, M., and Jaitly, N. Pointer networks. In Cortes, C., Lawrence, N. D., Lee, D. D., Sugiyama, M., and Garnett, R. (eds.), *Advances in Neural Information Processing Systems 28: Annual Conference on Neural Information Processing Systems 2015, December 7-12, 2015, Montreal, Quebec, Canada*, pp. 2692–2700, 2015. URL <https://proceedings.neurips.cc/paper/2015/hash/29921001f2f04bd3baee84a12e98098f-Abstract.html>.
- [72] Vinyals, O., Bengio, S., and Kudlur, M. Order matters: Sequence to sequence for sets. In Bengio, Y. and LeCun, Y. (eds.), *4th International Conference on Learning Representations, ICLR 2016, San Juan, Puerto Rico, May 2-4, 2016, Conference Track Proceedings*, 2016. URL <http://arxiv.org/abs/1511.06391>.
- [73] von Kügelgen, J., Ustyuzhaninov, I., Gehler, P., Bethge, M., and Schölkopf, B. Towards causal generative scene models via competition of experts. *ArXiv preprint*, abs/2004.12906, 2020. URL <https://arxiv.org/abs/2004.12906>.
- [74] Watters, N., Matthey, L., Bosnjak, M., Burgess, C. P., and Lerchner, A. COBRA: data-efficient model-based rl through unsupervised object discovery and curiosity-driven exploration. *ArXiv preprint*, abs/1905.09275, 2019. URL <https://arxiv.org/abs/1905.09275>.
- [75] Watters, N., Matthey, L., Burgess, C. P., and Lerchner, A. Spatial broadcast decoder: A simple architecture for learning disentangled representations in vaes. *ArXiv preprint*, abs/1901.07017, 2019. URL <https://arxiv.org/abs/1901.07017>.

- [76] Yu, H.-X., Guibas, L. J., and Wu, J. Unsupervised discovery of object radiance fields. *ArXiv preprint*, abs/2107.07905, 2021. URL <https://arxiv.org/abs/2107.07905>.
- [77] Yuan, J., Li, B., and Xue, X. Unsupervised learning of compositional scene representations from multiple unspecified viewpoints. *ArXiv preprint*, abs/2112.03568, 2021. URL <https://arxiv.org/abs/2112.03568>.
- [78] Yuille, A. and Kersten, D. Vision as bayesian inference: analysis by synthesis? *Trends in cognitive sciences*, 10(7):301–308, 2006.
- [79] Zablotkskaia, P., Dominici, E. A., Sigal, L., and Lehrmann, A. M. PROVIDE: a probabilistic framework for unsupervised video decomposition. In *Uncertainty in Artificial Intelligence*, pp. 2019–2028. PMLR, 2021.
- [80] Zaheer, M., Kottur, S., Ravanbakhsh, S., Póczos, B., Salakhutdinov, R., and Smola, A. J. Deep sets. In Guyon, I., von Luxburg, U., Bengio, S., Wallach, H. M., Fergus, R., Vishwanathan, S. V. N., and Garnett, R. (eds.), *Advances in Neural Information Processing Systems 30: Annual Conference on Neural Information Processing Systems 2017, December 4-9, 2017, Long Beach, CA, USA*, pp. 3391–3401, 2017. URL <https://proceedings.neurips.cc/paper/2017/hash/f22e4747da1aa27e363d86d40ff442fe-Abstract.html>.
- [81] Zhang, Y., Hare, J. S., and Prügel-Bennett, A. Learning representations of sets through optimized permutations. In *7th International Conference on Learning Representations, ICLR 2019, New Orleans, LA, USA, May 6-9, 2019*. OpenReview.net, 2019. URL <https://openreview.net/forum?id=HJMccjAcYX>.
- [82] Zhu, Y., Gao, T., Fan, L., Huang, S., Edmonds, M., Liu, H., Gao, F., Zhang, C., Qi, S., Wu, Y. N., et al. Dark, beyond deep: A paradigm shift to cognitive ai with humanlike common sense. *Engineering*, 6(3):310–345, 2020.
- [83] Zoran, D., Kabra, R., Lerchner, A., and Rezende, D. J. PARTS: unsupervised segmentation with slots, attention and independence maximization. In *Proceedings of the IEEE/CVF International Conference on Computer Vision*, pp. 10439–10447, 2021.

A Appendix

A.1 Matching Pseudocode

Algorithm 1 Greedy approximate matching. Uses $O(K)$ time and $O(K^2)$ space.

```

1: Input: Randomly ordered segregation posterior means  $\mu_{o_{1:K}}$ , imagination rollout means  $\mu_{\pi_{1:K}}$ 
2:  $C[i, j] = \|\mu_{\pi_i} - \mu_{o_j}\|_2, \forall i, j = 1, \dots, K$ 
3:  $\sigma := \text{zeros}(K, K)$ 
4: for index  $i = 0 \dots K - 1$  do
5:    $j^* = \arg \min C[i, :]$ 
6:    $C[:, j^*] = + \infty$ 
7:    $\sigma[j^*, i] = 1$ 
8: end for
9: return Permutation  $\sigma$ 

```

Alternative matching algorithms such as the Hungarian algorithm [50] can be used instead at a higher computational cost; however, we leave an empirical comparison of these algorithms for future work.

A.2 SRI Inference Pseudocode

Algorithm 2 SRI Inference. All sampling uses the Gaussian reparameterization trick [38].

```

1: Input: Scene observation  $\mathbf{x}$ , segregation VAE encoder  $e_\psi(\mathbf{x})$ , scene-level encoder  $f_\phi(\mathbf{z})$ , autoregressive prior  $\text{LSTM}_\theta$ , autoregressive posterior  $\text{LSTM}_\phi$ 
2:  $\mathbf{z}_{o_{1:K}} \sim q_\psi(\mathbf{z}_{o_{1:K}} | \mathbf{x}) \leftarrow e_\psi(\mathbf{x})$  /* Segregate */
3:  $\mathbf{s} \sim q_\phi(\mathbf{s} | \mathbf{x}) \leftarrow f_\phi(\mathbf{z}_{o_{1:K}})$  /* Relate */
4:  $\mathbf{z}_{\pi_1} \sim p_\theta(\mathbf{z}_{\pi_1} | \mathbf{s}) \leftarrow \text{LSTM}_\theta(\{\mathbf{s}\})$  /* Imagine */
5:  $\mathbf{z}_{\pi_k} \sim p_\theta(\mathbf{z}_{\pi_k} | \mathbf{z}_{\pi_{1:k-1}}, \mathbf{s}) \leftarrow \text{LSTM}_\theta(\{\mathbf{s}, \mathbf{z}_{\pi_{1:k-1}}\})$  for all  $k = 2, \dots, K - 1$ 
6:  $\sigma \leftarrow \text{Matching}(\mathbf{z}_{o_{1:K}}, \mathbf{z}_{\pi_{1:K}})$  /* we pass the posterior means to Algorithm 1 */
7:  $\mu_{o_{1:K}} \xrightarrow{\sigma} \mu_{\hat{\pi}_{1:K}}$  /* apply the permutation to the  $K$  means of  $q_\phi(\mathbf{z}_{o_{1:K}} | \mathbf{x})$  */
8:  $\bar{\sigma}_{\hat{\pi}_1}^2 \leftarrow \text{LSTM}_\phi(\{\mathbf{s}\})$  /* predict new correlated variances */
9:  $\bar{\sigma}_{\hat{\pi}_k}^2 \leftarrow \text{LSTM}_\phi(\{\mathbf{s}, \mu_{\hat{\pi}_{1:k-1}}\})$  for all  $k = 2, \dots, K - 1$ 
10:  $q_\phi(\mathbf{z}_{\hat{\pi}_{1:K}} | \mathbf{s}, \mathbf{x}) := \prod_{k=1}^K \mathcal{N}(\mu_{\hat{\pi}_k}, \bar{\sigma}_{\hat{\pi}_k}^2)$  /* autoregressive slot posterior */
11: return The sufficient statistics (e.g., means and variances) for the segregation posterior  $q_\psi(\mathbf{z}_{o_{1:K}} | \mathbf{x})$ , scene posterior  $q_\phi(\mathbf{s} | \mathbf{x})$ , autoregressive slot posterior  $q_\phi(\mathbf{z}_{\hat{\pi}_{1:K}} | \mathbf{s}, \mathbf{x})$ 

```

Our proposed set-to-sequence slot inference involves *aligning* the object order of the segregation posterior to the learned object generation order (Lines 6-7) and then transforming this posterior into an autoregressive distribution by predicting a sequence of correlated variances (Lines 8-10).

A.3 ELBO Derivation

We derive a lower bound on the log marginal scene likelihood as follows:

$$\log p(\mathbf{x}) = \log \int p_\theta(\mathbf{x}, \mathbf{s}, \mathbf{z}_{\pi_{1:K}}) d\mathbf{s}, d\mathbf{z}_{\pi_{1:K}} \quad (16)$$

$$= \log \int \frac{q_\phi(\mathbf{s}, \mathbf{z}_{\pi_{1:K}} | \mathbf{x})}{q_\phi(\mathbf{s}, \mathbf{z}_{\pi_{1:K}} | \mathbf{x})} p_\theta(\mathbf{x}, \mathbf{s}, \mathbf{z}_{\pi_{1:K}}) d\mathbf{s}, d\mathbf{z}_{\pi_{1:K}} \quad (17)$$

$$= \log \mathbb{E}_{q_\phi(\mathbf{s}, \mathbf{z}_{\pi_{1:K}} | \mathbf{x})} \left[\frac{p_\theta(\mathbf{x}, \mathbf{s}, \mathbf{z}_{\pi_{1:K}})}{q_\phi(\mathbf{s}, \mathbf{z}_{\pi_{1:K}} | \mathbf{x})} \right]. \quad (18)$$

Applying Jensen's inequality and then factorizing gives:

$$\log p(\mathbf{x}) \geq \mathbb{E}_{q_\phi(\mathbf{s}, \mathbf{z}_{\pi_{1:K}} | \mathbf{x})} \left[\log \frac{p_\theta(\mathbf{x}, \mathbf{s}, \mathbf{z}_{\pi_{1:K}})}{q_\phi(\mathbf{s}, \mathbf{z}_{\pi_{1:K}} | \mathbf{x})} \right] \quad (19)$$

$$= \mathbb{E}_{q_\phi(\mathbf{s} | \mathbf{x})} \left[\mathbb{E}_{q_\phi(\mathbf{z}_{\pi_{1:K}} | \mathbf{s}, \mathbf{x})} \left[\log \frac{p(\mathbf{s}) p_\theta(\mathbf{z}_{\pi_{1:K}} | \mathbf{s}) p_\theta(\mathbf{x} | \mathbf{z}_{\pi_{1:K}})}{q_\phi(\mathbf{s} | \mathbf{x}) q_\phi(\mathbf{z}_{\pi_{1:K}} | \mathbf{s}, \mathbf{x})} \right] \right]. \quad (20)$$

We use the fact that $\log(\frac{A}{B/D}) = \log(\frac{A}{B}) + \log(\frac{C}{D})$ to factor Eq. 20 into a sum of three losses. The autoregressive slot posterior order obtained for inference $\hat{\pi}_{1:K}$ is shown in blue.

The first term is a negative log-likelihood loss:

$$\mathcal{L}_{\text{NLL}} = -\mathbb{E}_{q_\phi(\mathbf{s}|\mathbf{x})} \left[\mathbb{E}_{q_\phi(\mathbf{z}_{\hat{\pi}_{1:K}}|\mathbf{s},\mathbf{x})} [\log p_\theta(\mathbf{x} | \mathbf{z}_{\hat{\pi}_{1:K}})] \right]. \quad (21)$$

The second is a slot-level reverse KL loss with the approximate order:

$$\mathcal{L}_{\text{slotKL}} = -\mathbb{E}_{q_\phi(\mathbf{s}|\mathbf{x})} \left[\mathbb{E}_{q_\phi(\mathbf{z}_{\hat{\pi}_{1:K}}|\mathbf{s},\mathbf{x})} \left[\log \frac{p_\theta(\mathbf{z}_{\hat{\pi}_{1:K}} | \mathbf{s})}{q_\phi(\mathbf{z}_{\hat{\pi}_{1:K}} | \mathbf{s}, \mathbf{x})} \right] \right] \quad (22)$$

$$= \mathbb{E}_{q_\phi(\mathbf{s}|\mathbf{x})} \left[\mathbb{E}_{q_\phi(\mathbf{z}_{\hat{\pi}_{1:K}}|\mathbf{s},\mathbf{x})} \left[\log \frac{q_\phi(\mathbf{z}_{\hat{\pi}_{1:K}} | \mathbf{s}, \mathbf{x})}{p_\theta(\mathbf{z}_{\hat{\pi}_{1:K}} | \mathbf{s})} \right] \right] \quad (23)$$

$$= \mathbb{E}_{q_\phi(\mathbf{s}|\mathbf{x})} \left[\sum_{k=1}^K \mathbb{E}_{q_\phi(\mathbf{z}_{\hat{\pi}_{1:k}}|\mathbf{s},\mathbf{x})} \left[\log \frac{q_\phi(\mathbf{z}_{\hat{\pi}_k} | \mathbf{z}_{\hat{\pi}_{1:k-1}}, \mathbf{s}, \mathbf{x})}{p_\theta(\mathbf{z}_{\hat{\pi}_k} | \mathbf{z}_{\hat{\pi}_{1:k-1}}, \mathbf{s})} \right] \right] \quad (24)$$

$$= \mathbb{E}_{q_\phi(\mathbf{s}|\mathbf{x})} [D_{KL}(q_\phi(\mathbf{z}_{\hat{\pi}_1} | \mathbf{s}, \mathbf{x}) \| p_\theta(\mathbf{z}_{\hat{\pi}_1} | \mathbf{s}))] \quad (25)$$

$$+ \mathbb{E}_{q_\phi(\mathbf{s}|\mathbf{x})} \left[\sum_{k=2}^K \mathbb{E}_{q_\phi(\mathbf{z}_{\hat{\pi}_{1:k-1}}|\mathbf{s},\mathbf{x})} [D_{KL}(q_\phi(\mathbf{z}_{\hat{\pi}_k} | \mathbf{z}_{\hat{\pi}_{1:k-1}}, \mathbf{s}, \mathbf{x}) \| p_\theta(\mathbf{z}_{\hat{\pi}_k} | \mathbf{z}_{\hat{\pi}_{1:k-1}}, \mathbf{s}))] \right]. \quad (26)$$

The third term is a scene-level reverse KL loss:

$$\mathcal{L}_{\text{sceneKL}} = -\mathbb{E}_{q_\phi(\mathbf{s}|\mathbf{x})} \left[\mathbb{E}_{q_\phi(\mathbf{z}_{\pi_{1:K}}|\mathbf{s},\mathbf{x})} \left[\log \frac{p(\mathbf{s})}{q_\phi(\mathbf{s} | \mathbf{x})} \right] \right] \quad (27)$$

$$= -\mathbb{E}_{q_\phi(\mathbf{s}|\mathbf{x})} \left[\log \frac{p(\mathbf{s})}{q_\phi(\mathbf{s} | \mathbf{x})} \right] \quad (28)$$

$$= \mathbb{E}_{q_\phi(\mathbf{s}|\mathbf{x})} \left[\log \frac{q_\phi(\mathbf{s} | \mathbf{x})}{p(\mathbf{s})} \right] \quad (29)$$

$$= D_{KL}(q_\phi(\mathbf{s} | \mathbf{x}) \| p(\mathbf{s})). \quad (30)$$

We also define an auxiliary slot-level reverse KL loss similar to Eq. 26 except that the inner expectation is now taken with respect to the slot posterior and the K -step rollout with order $\pi_{1:K}$:

$$\mathcal{L}_{\text{rolloutKL}} = \mathbb{E}_{q_\phi(\mathbf{s}|\mathbf{x})} [D_{KL}(q_\phi(\mathbf{z}_{\hat{\pi}_1} | \mathbf{s}, \mathbf{x}) \| p_\theta(\mathbf{z}_{\pi_1} | \mathbf{s}))] \quad (31)$$

$$+ \mathbb{E}_{q_\phi(\mathbf{s}|\mathbf{x})} \left[\sum_{k=2}^K \mathbb{E}_{q_\phi(\mathbf{z}_{\hat{\pi}_{1:k-1}}|\mathbf{s},\mathbf{x})} \left[\mathbb{E}_{p_\theta(\mathbf{z}_{\pi_{1:k-1}}|\mathbf{s})} [D_{KL}(q_\phi(\mathbf{z}_{\hat{\pi}_k} | \star) \| p_\theta(\mathbf{z}_{\pi_k} | \star))] \right] \right], \quad (32)$$

where $q_\phi(\mathbf{z}_{\hat{\pi}_k} | \star) := q_\phi(\mathbf{z}_{\hat{\pi}_k} | \mathbf{z}_{\hat{\pi}_{1:k-1}}, \mathbf{s}, \mathbf{x})$ and $p_\theta(\mathbf{z}_{\pi_k} | \star) := p_\theta(\mathbf{z}_{\pi_k} | \mathbf{z}_{\pi_{1:k-1}}, \mathbf{s})$. The auxiliary KL term is always non-negative by definition, so adding it to the negative ELBO only increases the upper bound on $-\log p(\mathbf{x})$ (equivalently, loosens the lower bound on $\log p(\mathbf{x})$). Summed together, the four terms form the SRI loss: $\mathcal{L}_{\text{SRI}} = \mathcal{L}_{\text{NLL}} + \mathcal{L}_{\text{slotKL}} + \mathcal{L}_{\text{rolloutKL}} + \mathcal{L}_{\text{sceneKL}}$. In practice, we approximate the expectations with a single sample and average the loss over a minibatch of size $B = 32$ of dataset samples. We leave a formal characterization of how the accuracy of the matching between $\hat{\pi}$ and π affects the lower bound on the marginal log likelihood for future work. Intuitively, as long as the two slot orders are ‘‘close’’, we can expect these lower bounds to be similar as well.

A.4 Experiment details

A.4.1 Hyperparameters

Architecture: We use $|\mathbf{z}_k| = 64$ for all environments following GENv2 and EMORL. We set $|\mathbf{s}| = 128$ to be twice the slot dimension. The number of attention layers for scene posterior estimation is fixed at $L = 3$; we found that varying L incurred little change in performance. We use the same hyperparameters for the image encoder and decoder architectures as used by GENv2 and EMORL for SRI-X and SRI-EMORL, respectively. Both of the GENv2 and EMORL implementations

are based on open source released by the respective authors.^{2,3} For SRI-EMORL we fix the number of iterative refinement steps to 2. Following GEN and GENv2, SRI’s autoregressive prior and posterior LSTM uses 256 hidden units. When training GENv2 jointly with SRI we replace its autoregressive prior with a slot-wise independent prior. SRI uses GELU non-linear activations [26] after each linear projection of the scene variable and in the attention layers. All layers use Xavier weight initialization [18].

Optimization: We mostly adopt the same hyperparameters here as used by GENv2 and EMORL. SRI based on GENv2 uses the Adam optimizer [37] with default hyperparameters and a learning rate of 1e-4 but without any learning rate schedule. SRI-EMORL uses an initial learning rate of 4e-4, grad norm clipping to 5, and learning rate schedule consisting of a linear warmup for 10K steps then multiplicative decay with by a rate of 0.5 every 100K steps. A batch size of 32 is used for all models. Both GENv2 and EMORL use GECO to balance reconstruction and KL during optimization; we discuss the GECO hyperparameters in Section A.4.2.

Datasets: Both CLEVR6 and Objects Room can be accessed freely online under the Apache License 2.0.⁴ The ShapeStacks dataset is also freely available for download online under the GNU License 3.0.⁵ We use the same preprocessing protocol for CLEVR6 as Emami et al. [14], which is to center crop the images to 192x192 and the resize them to size 96x96. Objects Room and ShapeStacks have 64x64 RGB images.

A.4.2 Balancing reconstruction and KL with GECO

Both GENv2 and EMORL use GECO to balance reconstruction and KL losses [58]. Each code base has its own GECO implementation and GECO hyperparameter schedule which we use to train SRI-X and SRI-EMORL.

SRI-G (unnormalized Gaussian image likelihood and global $\sigma = 0.7$) uses a per-pixel and per-channel GECO target of -0.353 on Objects Room and ShapeStacks and -0.356 on CLEVR6. We decreased the GECO learning rate from 1e-5 to 1e-6. Once the GECO target is reached the learning rate is multiplied by a speedup factor of 10 to accelerate the decay of the GECO Lagrange parameter.

SRI-MoG uses the same GECO hyperparameters as GENv2-MoG on ShapeStacks and Objects Room (target is 0.5655—note that the MoG likelihood here is normalized) except we also use the decreased GECO learning rate of 1e-6. However, on Objects Room we notice that this increased training instability, likely because this warms up the KL less aggressively than the faster GECO learning rate does. We use restarting from model checkpoints to mitigate this here.

For SRI-EMORL on CLEVR6 we used a target of -2.265 for unnormalized Gaussian image likelihood with global $\sigma = 0.1$. The rule of thumb used to tune the GECO target is that the target should be reached after about 20% of the training steps. This gives ample time for the GECO Lagrange parameter to automatically decay back to 1 so that a valid ELBO is eventually maximized. We use a GECO learning rate of 1e-6 and speedup of 10 as well.

A.4.3 Baselines and compute

GENESIS and GENESIS-v2: The authors of GENv2 have released pre-trained weights for GEN trained on ShapeStacks and GENv2-MoG trained on Objects Room and ShapeStacks. We use these weights for model visualizations and to compute the structure accuracy metric. To train GENv2-MoG on CLEVR6 we had to lower the standard deviation to 0.1. We adjusted the GENv2-MoG GECO target accordingly by tuning it to -2.265. To compute the FID score, we follow the same protocol as GENv2 [16] and use 10K real and generated samples.

GNM: We use the official GNM PyTorch implementation provided by the authors.⁶ We train GNM on the 128x128 resolution version of CLEVR6 so that we could use the default GNM hyperparameters that the authors used for the 128x128 resolution CLEVR-based environment from their paper. This worked well for CLEVR6. By default, GNM organizes its symbolic variables into a 4x4 spatial

²<https://github.com/pemami4911/EfficientMORL>

³<https://github.com/applied-ai-lab/genesis>

⁴https://github.com/deepmind/multi_object_datasets

⁵<https://ogroth.github.io/shapestacks/>

⁶<https://github.com/JindongJiang/GNM>

grid, which we maintained. We treat each spatial grid cell as one slot for a total of 16 slots. To train GNM on the 64x64 Objects Room and ShapeStacks scenes, we removed one downsampling and one upsampling layer from the encoder and decoder to account for the resolution being one-half that of CLEVR6. For all environments, we used the default global latent dim of 32 and z_{what} dim of 64.

Compute: In general, the majority of the compute is taken up by the segregation VAE (GENv2 and EMORL in this work). SRI adds a few lightweight neural networks and therefore only marginally increases training time.

- On Objects Room and ShapeStacks, SRI-X takes about 20 hours to reach 500K steps using 2 NVIDIA A100 GPUs. On CLEVR6, it about 24 hours to reach 425K steps, at which point we stopped training since the model showed signs of convergence and so as to keep training times at about one day or faster on equivalent hardware to ease reproducibility.
- The GENv2 and GEN baselines are negligibly faster to train. We train these baselines using the same setup as SRI.
- SRI-EMORL uses 8 NVIDIA A100 GPUs to reach 225K CLEVR6 which takes about 27 hours, at which point we cut off training to keep a similar compute budget to SRI with GENv2. The memory footprint of the two steps of iterative refinement used to estimate the segregation posterior is large, hence the need for 8 GPUs.
- GNM takes about 9 hours to reach 500K steps with a batch size of 32 on one A100 GPU for Objects Room and ShapeStacks. It takes about 12 hours to reach 500K steps on CLEVR6 on one A100 GPU.

A.4.4 Open source software

This project was conducting using the following open source Python packages: PyTorch [54], numpy [25], jupyter [39], matplotlib [31], scikit-learn [55], and sacred [20].

A.5 Additional Qualitative Results

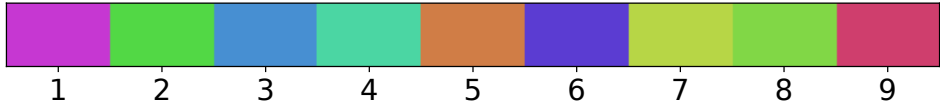


Figure 6: Mask color to slot number legend

Additional random samples: We visualize extra randomly sampled scenes from SRI-MoG (Figure 7), SRI-G (Figure 8), and GENv2-G (Figure 9).

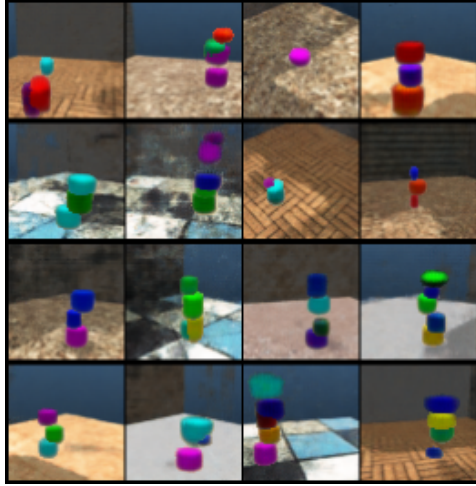
Generalizing to different numbers of slots: We demonstrate that the number of slots can be changed at test time to generate scenes with fewer or more objects than seen during training in Figure 10.

Effect of temperature scaling: We investigate whether temperature scaling provides any further qualitative improvement in sample quality (Figure 11).

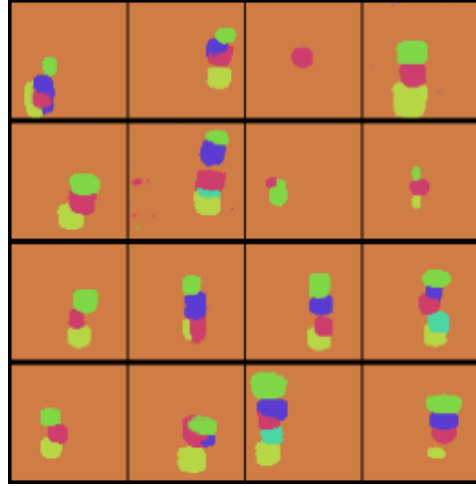
Random samples from SRI-EMORL: Random samples from SRI-EMORL on CLEVR6 (visualized with temperature scaling) (Figure 12).

Imagination rollouts: We provide more examples of pairs of reconstructed scenes with the corresponding imagination rollout used by SRI for slot order estimation (Figure 13).

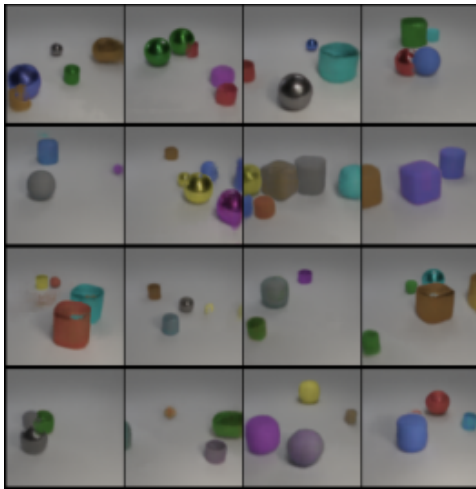
Reconstruction and segmentation examples: Examples of reconstructed and segmented scenes from each dataset for SRI-MoG (Figure 14), SRI-G (Figure 15), GENv2-G (Figure 16), and GNM (Figure 17).



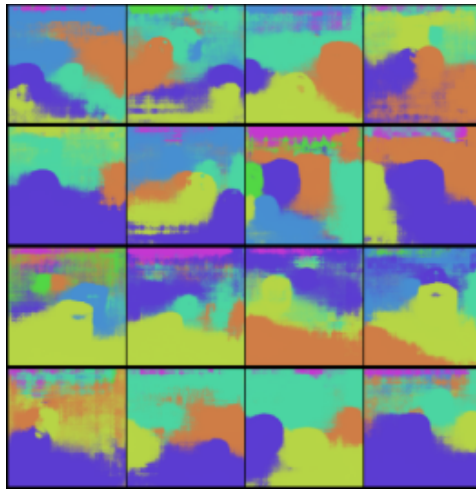
(a) ShapeStacks images



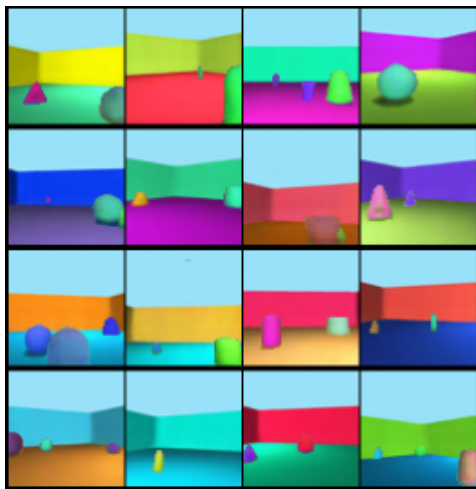
(b) ShapeStacks masks



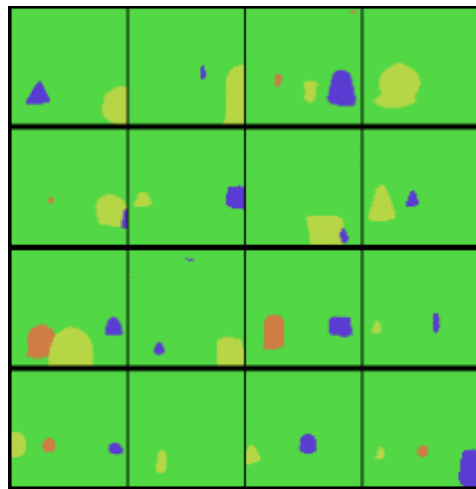
(c) CLEVR6 images



(d) CLEVR6 masks

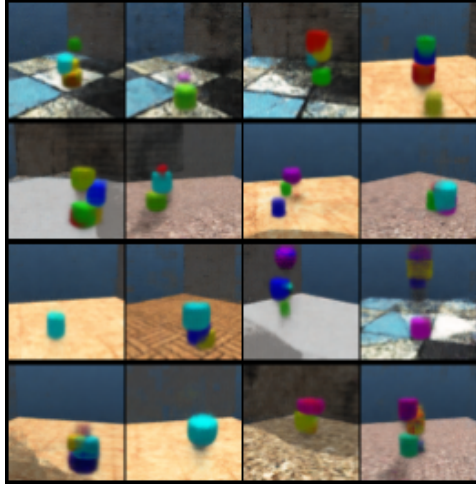


(e) Objects Room images

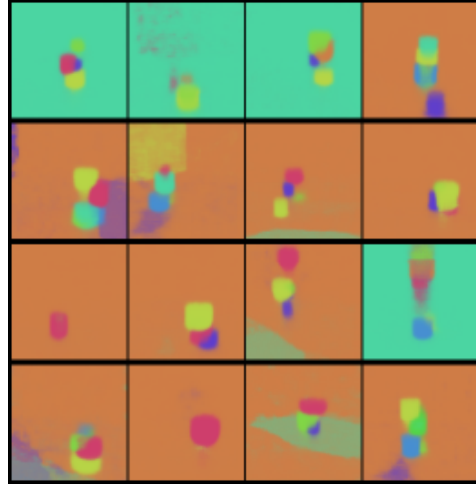


(f) Objects Room masks

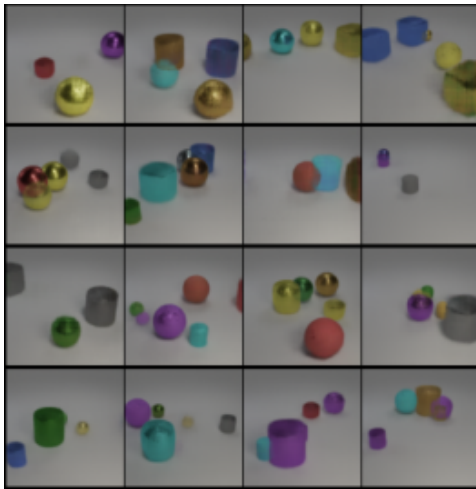
Figure 7: Additional random samples generated by SRI-MoG.



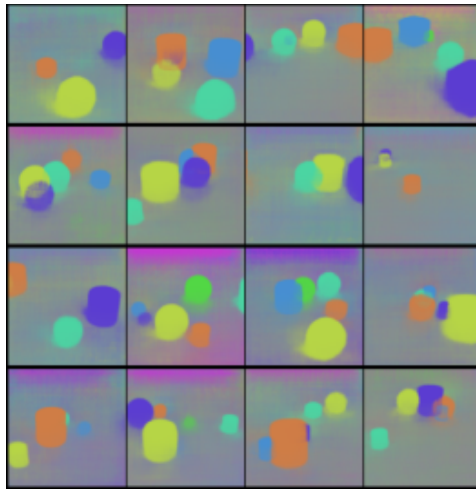
(a) ShapeStacks images



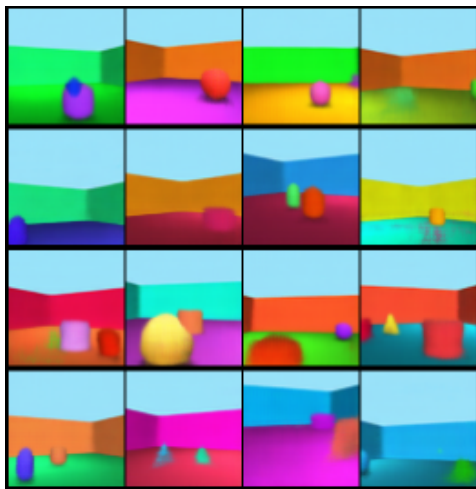
(b) ShapeStacks masks



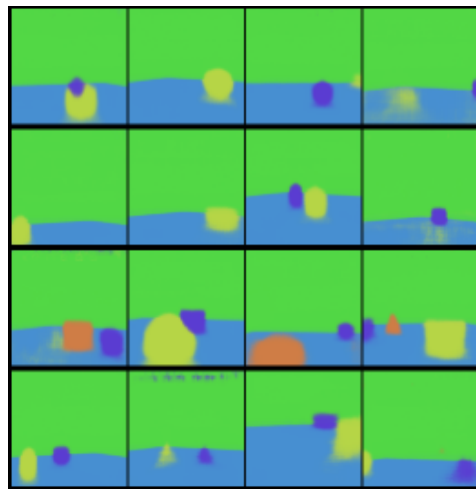
(c) CLEVR6 images



(d) CLEVR6 masks

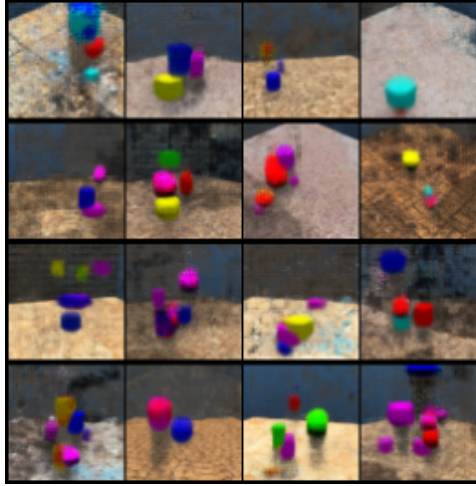


(e) Objects Room images

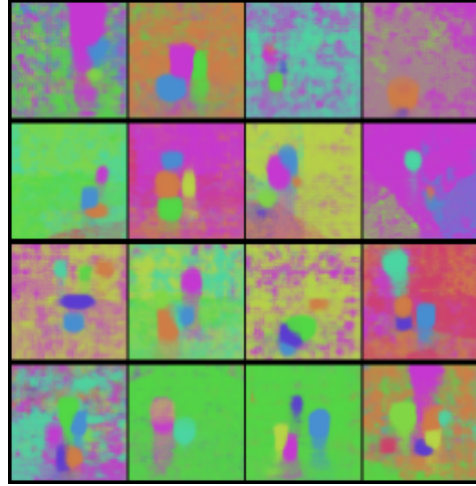


(f) Objects Room masks

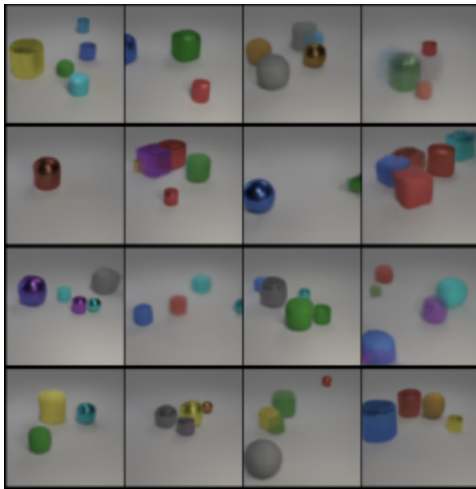
Figure 8: Additional random samples generated by SRI-G.



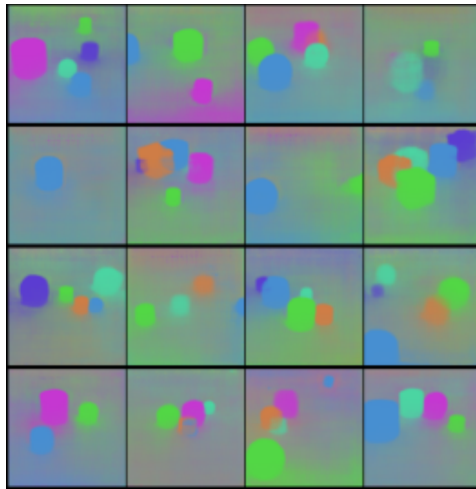
(a) ShapeStacks images



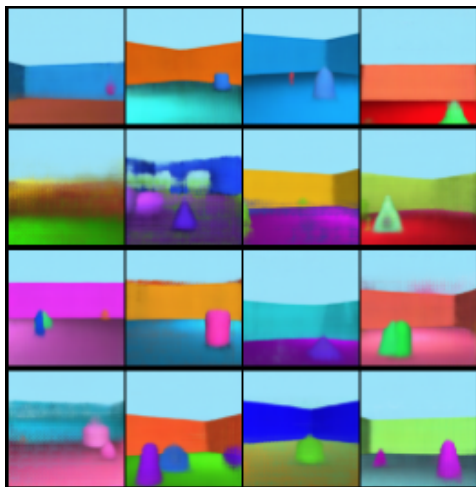
(b) ShapeStacks masks



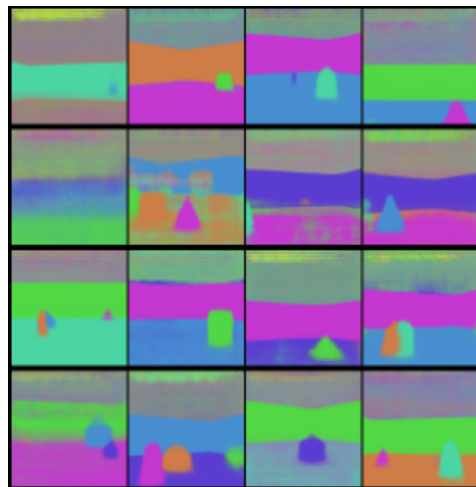
(c) CLEVR6 images



(d) CLEVR6 masks



(e) Objects Room images



(f) Objects Room masks

Figure 9: Additional random samples generated by GENESISv2-G.

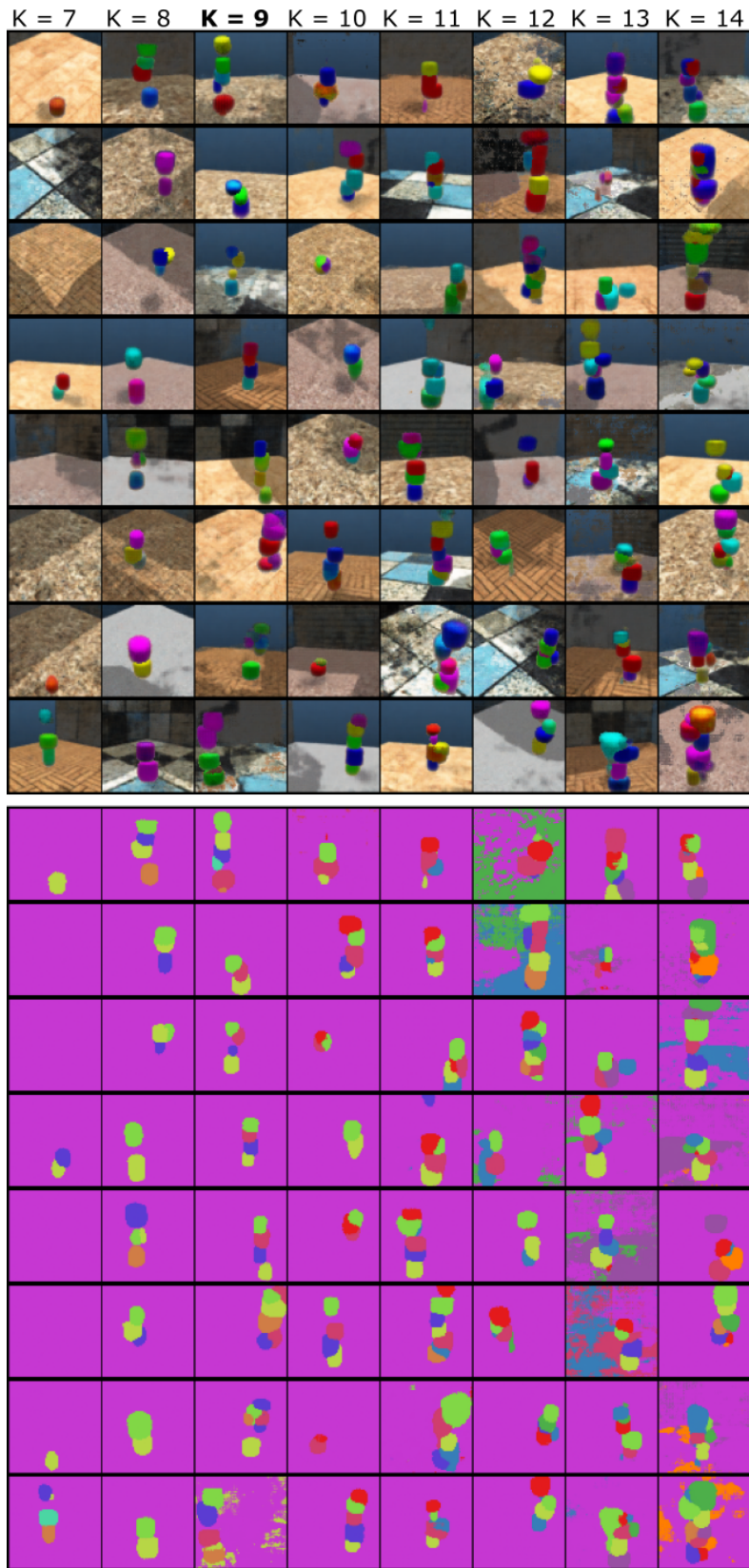


Figure 10: **Generalization to different numbers of slots K .** Random ShapeStacks samples. SRI-MoG was trained with $K = 9$.

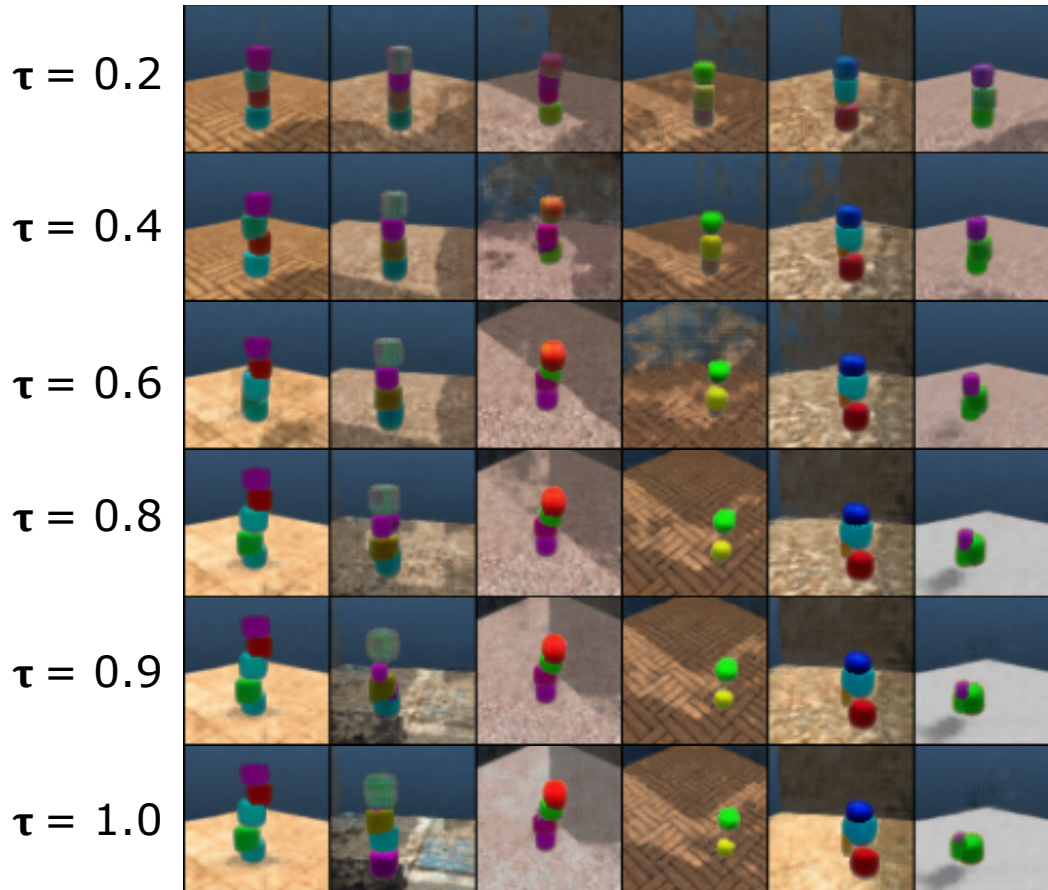
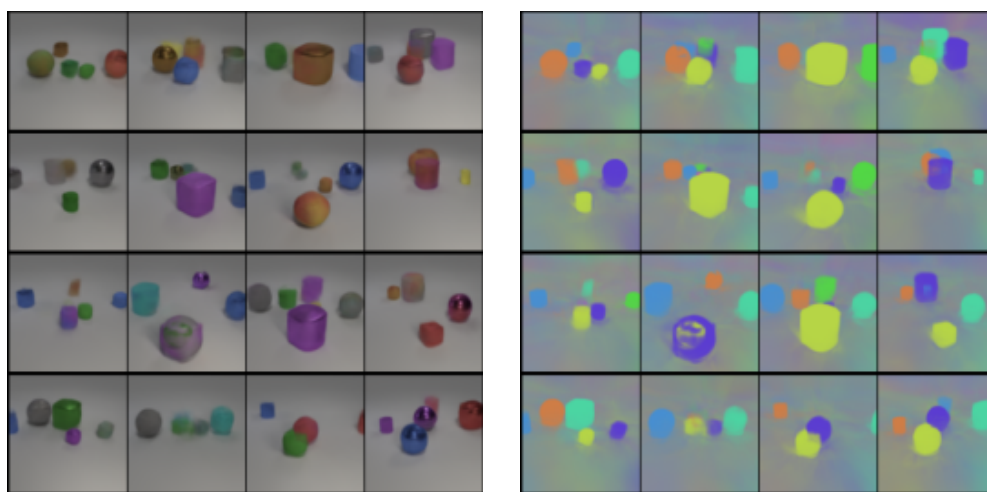


Figure 11: Randomly sampled ShapeStacks images from SRI-MoG with different temperature scaling parameters τ in the scene-level and slot prior. Scaling down the variances in a hierarchical Gaussian prior is known to help samples stay in regions of high probability [66]. We confirm here that values of τ near 1.0 slightly improve sample quality on challenging datasets with minimal impact on sample diversity. Note that we use $\tau = 1.0$ in this work for all evaluations unless stated otherwise.



(a) CLEVR6 images

(b) CLEVR6 masks

Figure 12: Random samples generated by SRI-EMORL. These images are generated with temperature $\tau = 0.8$.

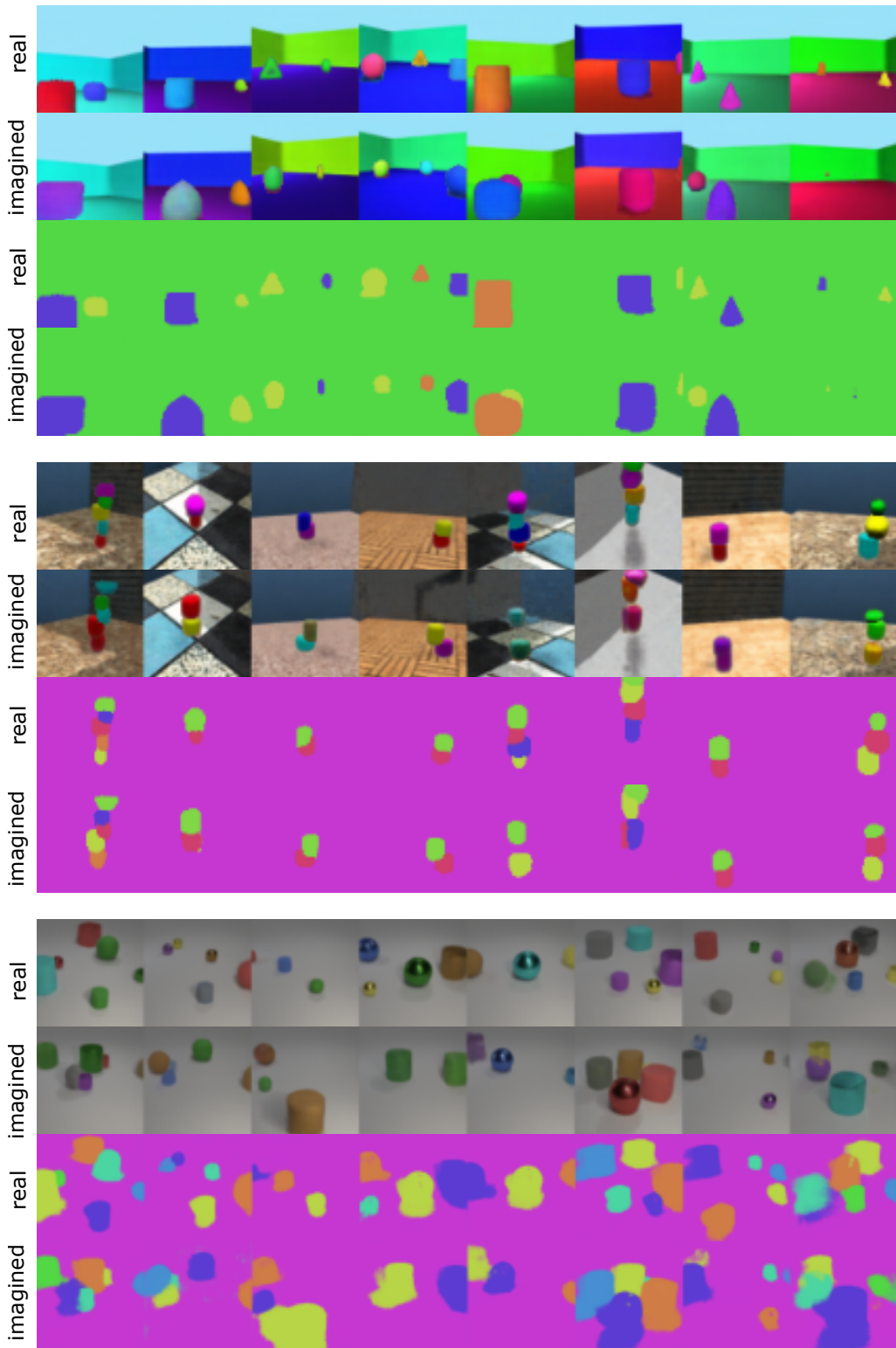


Figure 13: **Imagination examples.** Side-by-side comparisons of reconstructed RGB images and masks from SRI-MoG’s aligned autoregressive posterior with imagined RGB images and masks.

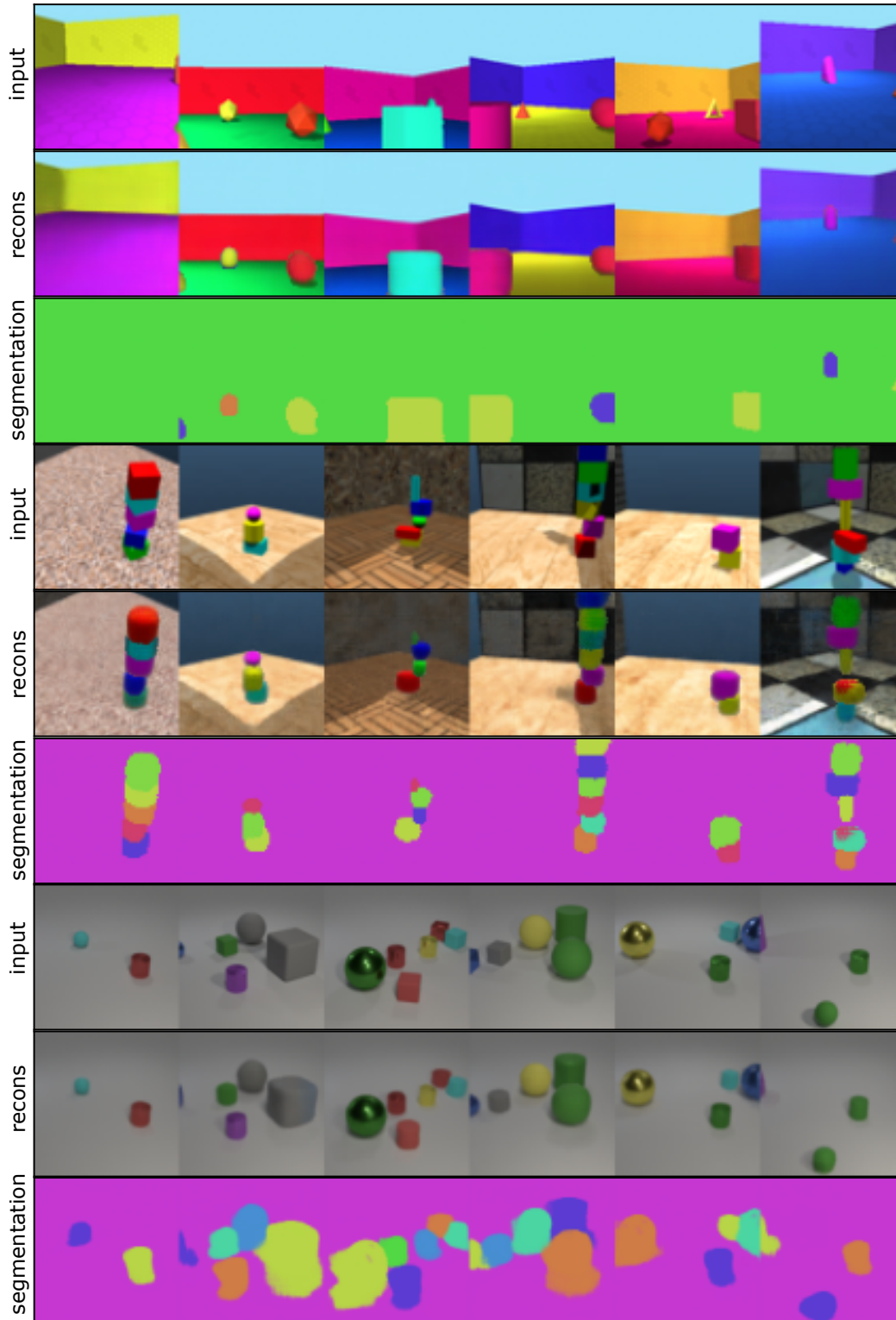


Figure 14: SRI-MoG reconstruction and segmentation.

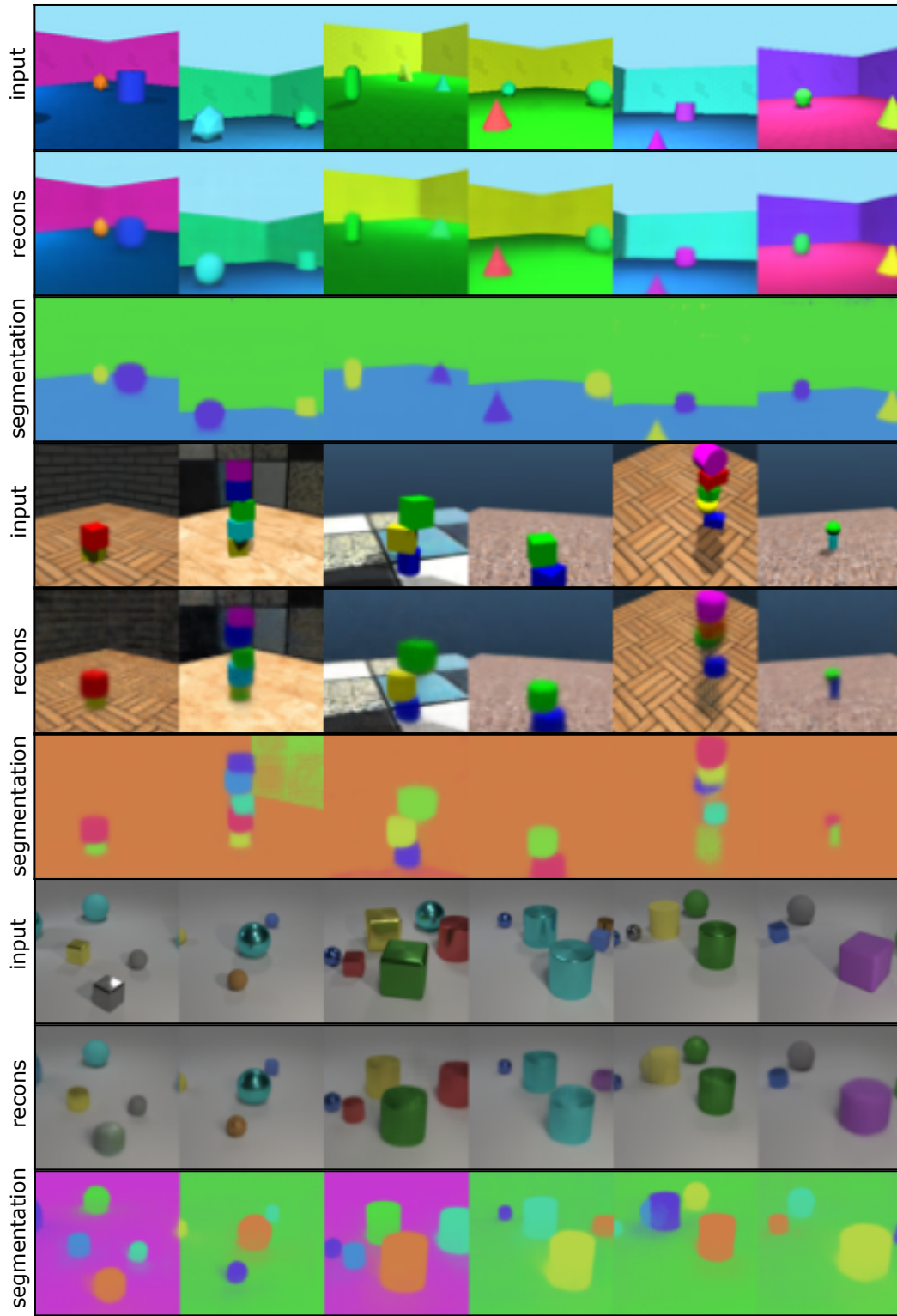


Figure 15: SRI-G reconstruction and segmentation.

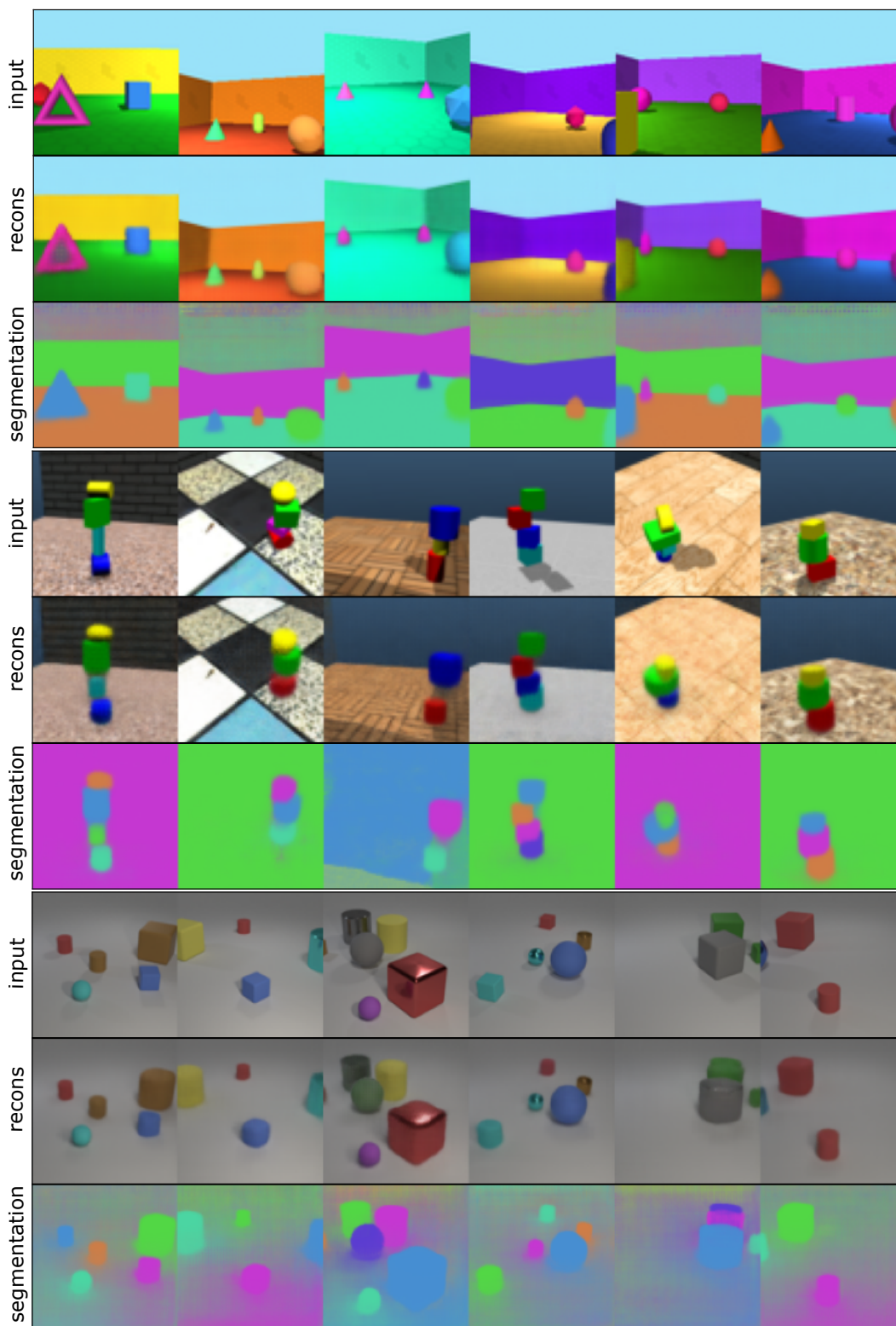


Figure 16: GENv2-G reconstruction and segmentation.

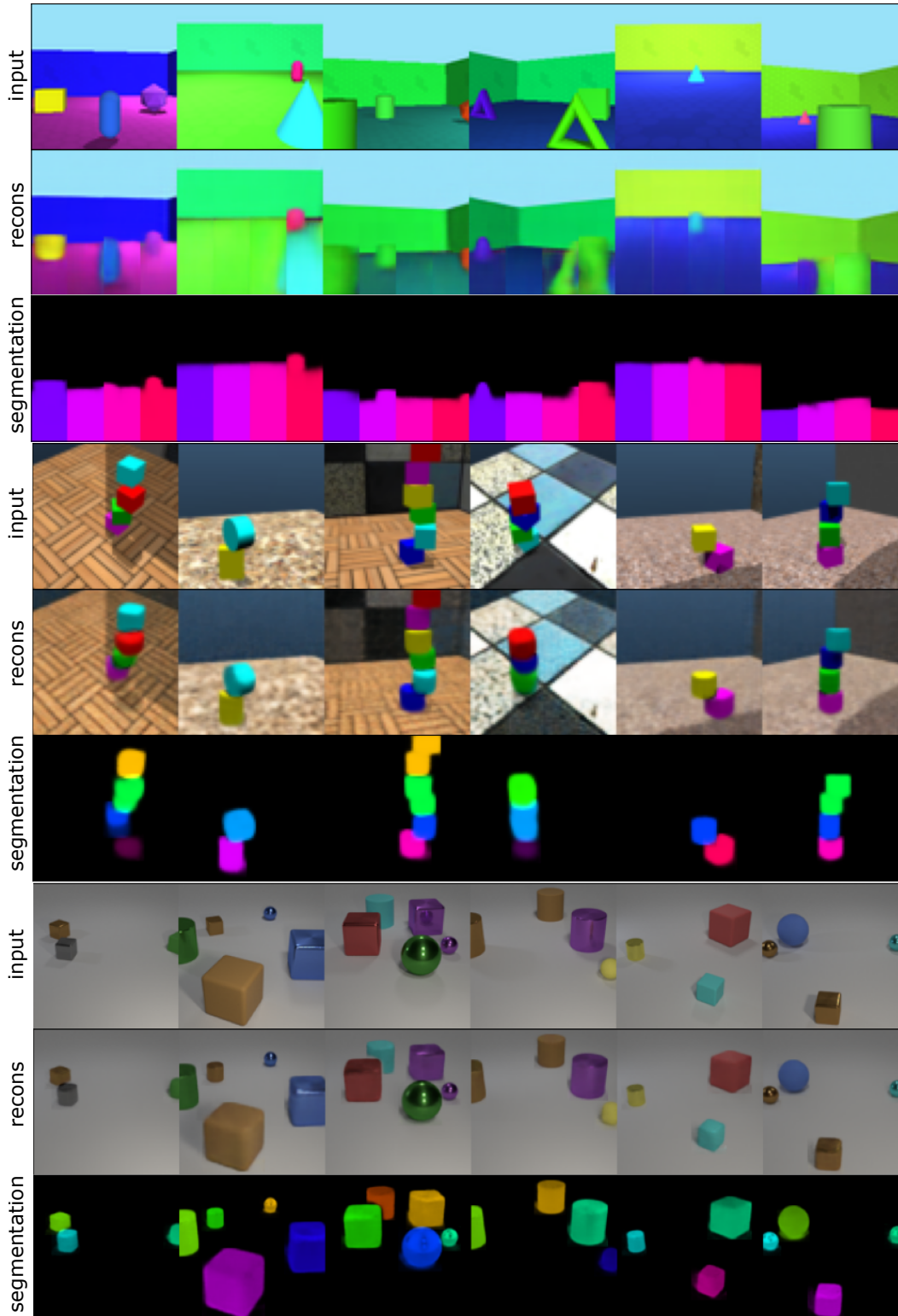


Figure 17: GNM reconstruction and segmentation. The symbolic variables, which are bound to a spatial grid of fixed resolution, are unable to properly bind to the foreground objects in the Objects Room and ShapeStacks datasets. In Objects Room, the shapes are segmented into strips and grouped with the ground. The wall is erroneously considered one of the foreground objects. In ShapeStacks, distinct blocks are segmented together when they fall within the same grid cell.